



---

MSU Graduate Theses

---

Summer 2021

## An Assessment of Inp/Zns as Potential Anti-Cancer Therapy: Quantum Dot Treatment Induces Stress on Hela Cells


Victoria Grace Davenport

Missouri State University, davenport17@live.missouristat.edu

As with any intellectual project, the content and views expressed in this thesis may be considered objectionable by some readers. However, this student-scholar's work has been judged to have academic value by the student's thesis committee members trained in the discipline. The content and views expressed in this thesis are those of the student-scholar and are not endorsed by Missouri State University, its Graduate College, or its employees.

---

Follow this and additional works at: <https://bearworks.missouristate.edu/theses>

 Part of the [Biology Commons](#), and the [Cell Biology Commons](#)

### Recommended Citation

Davenport, Victoria Grace, "An Assessment of Inp/Zns as Potential Anti-Cancer Therapy: Quantum Dot Treatment Induces Stress on Hela Cells" (2021). *MSU Graduate Theses*. 3639.  
<https://bearworks.missouristate.edu/theses/3639>

This article or document was made available through BearWorks, the institutional repository of Missouri State University. The work contained in it may be protected by copyright and require permission of the copyright holder for reuse or redistribution.

For more information, please contact [bearworks@missouristate.edu](mailto:bearworks@missouristate.edu).

**AN ASSESSMENT OF INP/ZNS AS POTENTIAL ANTI-CANCER THERAPY:  
QUANTUM DOT TREATMENT INDUCES STRESS ON HELA CELLS**

A Master's Thesis

Presented to

The Graduate College of  
Missouri State University

In Partial Fulfillment

Of the Requirements for the Degree  
Master of Science, Biology

By

Victoria Grace Davenport

May 2021

Copyright 2021 by Victoria Grace Davenport

# **AN ASSESSMENT OF INP/ZNS AS POTENTIAL ANTI-CANCER THERAPY: QUANTUM DOT TREATMENT INDUCES STRESS ON HELA CELLS**

Biology

Missouri State University, May 2021

Master of Science

Victoria Grace Davenport

## **ABSTRACT**

Indium Phosphide/Zinc Sulfide (InP/ZnS) quantum dots (QDs) are an emerging option in QD technologies for uses of fluorescent imaging as well as targeted drug and anti-cancer therapies based on their customizable properties. In this study we explored effects of InP/ZnS when treated with HeLa cervical cancer cells. We employed XTT viability assays, reactive oxygen species (ROS) analysis, and apoptosis analysis to better understand cytotoxicity extents at different concentrations of InP/ZnS. In addition, we compared the transcriptome profile from the QD-treated HeLa cells with that of untreated HeLa cells to identify changes to the transcriptome in response to the QD. Intracellular modes of action were illustrated. Our study determined both IC<sub>50</sub> concentration of 69  $\mu\text{g/mL}$  and MIC concentration of 167  $\mu\text{g/mL}$  of InP/ZnS. It was observed via XTT assay that cell viability decreased significantly at the MIC. In analysis of median fluorescent intensity (MFI) using ROS assay and flow cytometry, cells positive for producing both superoxide and peroxynitrite increased in intensity compared to the control. Using analysis of apoptosis, we found that induced cell death in the QD-treated samples was shown to be significantly increased when compared to untreated cells. We conclude InP/ZnS QD to decrease cell viability by inducing stress via ROS levels, apoptosis induction, and alteration of transcriptome.

**KEYWORDS:** quantum dot, HeLa, nanoparticle, cancer, apoptosis, genome, InP/ZnS

**AN ASSESSMENT OF INP/ZNS AS POTENTIAL ANTI-CANCER THERAPY:  
QUANTUM DOT TREATMENT INDUCES STRESS ON HELA CELLS**

By

Victoria Grace Davenport

A Master's Thesis  
Submitted to the Graduate College  
Of Missouri State University  
In Partial Fulfillment of the Requirements  
For the Degree of Master of Science, Biology

May 2021

Approved:

Kyoungtae Kim, Ph.D., Thesis Committee Chair

Christopher Lupfer, Ph.D., Committee Member

Ryan Udan, Ph.D., Committee Member

Julie Masterson, Ph.D., Dean of the Graduate College

In the interest of academic freedom and the principle of free speech, approval of this thesis indicates the format is acceptable and meets the academic criteria for the discipline as determined by the faculty that constitute the thesis committee. The content and views expressed in this thesis are those of the student-scholar and are not endorsed by Missouri State University, its Graduate College, or its employees.

## ACKNOWLEDGEMENTS

The journey to a master's degree and completion of a thesis is not an easy one. When they say, "it takes a village", they weren't lying. I have had a village of support on this journey that I am so grateful for. I first thank my university for the opportunity and community of staff and peers that come with it. To my mentor and advisor, Dr. Kim, I thank you for believing in me and giving continual support and expertise throughout this process. To my lab mates, I thank you for your constant willingness to lend a hand when I needed it. To my friends outside the realm of research, I am forever grateful for your unwavering loyalty and motivation; thank you for pushing me forward and being there when I stumbled. To my little sister, you are essential to me and my success. If I had to choose between being an only child or having 10 siblings, I'd want 10 copies of you. To my grandparents, if there is one place I can always count on for comfort and support it is with you all. Thank you for fiercely believing in me and never failing to show up. Finally, to my parents: I don't know if I'll ever be able to adequately show you how thankful I am for your undying support in everything I do, but know I love you unconditionally and forever.

I dedicate this thesis to my family.

## TABLE OF CONTENTS

Introduction	Page 1
Origin and Importance of HeLa Cells	Page 1
Overview of Quantum Dots Usage	Page 1
Customizable Properties of Quantum Dots	Page 2
Resulting Cytotoxicity with Quantum Dot Treatment	Page 5
InP Alternative to Cd Quantum Dot	Page 6
Problem Statement and Hypothesis	Page 7
Materials and Methods	Page 9
InP/ZnS Quantum Dots	Page 9
Cell Culture	Page 10
XTT Viability Assay	Page 10
Calculation of IC50 Value	Page 11
Reactive Oxygen Species Assay	Page 11
Apoptosis Assay	Page 12
Total RNA Extraction and cDNA Conversion	Page 13
RNA-seq Transcriptome Analysis	Page 13
Statistical Analysis	Page 14
Results	Page 15
Chemophysical Properties of Green InP/ZnS	Page 15
Effect on Cell Viability When Treated with InP/ZnS QD	Page 16
Increased Production of Superoxide and Peroxynitrite Radicals in InP/ZnS Presence	Page 17
Increased Late Apoptosis with InP/ZnS Treatment	Page 19
Altered Genome with InP/ZnS Treatment	Page 20
Discussion	Page 21
Changes to HeLa Cell Viability, ROS, and Apoptosis Levels with InP/ZnS Treatment	Page 21
Upregulated Gene Processes Increase ROS Production and Induce Apoptosis	Page 23
Downregulated Processes Also Prevent Tumor Growth Via Oxidative Stress	Page 25
Conclusion and Future Study	Page 29
References	Page 42

## LIST OF EQUATIONS

Equation 1. Inhibition Concentrations 50% (IC<sub>50</sub>)

Page 30



**LIST OF TABLES**

Table 1. Median Fluorescent Intensity

Page 31

## LIST OF FIGURES

Figure 1: STEM images	Page 32
Figure 2: EDAX spectra of InP/ZnS (530nm) QD	Page 33
Figure 3: Intensity size distribution	Page 34
Figure 4: UV-Vis absorption spectra	Page 35
Figure 5: UV (365nm) light excitation of InP/ZnS QDs 530nm (green)	Page 36
Figure 6, A and B: Cell viability visualized by XTT reagents after 7 hours of incubation with InP/ZnS QD.	Page 37
Figure 7: ROS measurements with both DHE and DHR at varied InP/ZnS QD concentrations.	Page 38
Figure 8: Levels of early and late apoptosis after InP/ZnS treatment.	Page 39
Figure 9: Altered up and down regulated processes	Page 40
Figure 10: Visualization of altered processes in the presence of InP/ZnS.	Page 41

## INTRODUCTION

### **Origin and Importance of the HeLa Cell**

HeLa cells are widely known for their advancements in medical research as well as their controversial origin. The cells were named after the woman from which they originated, taking the first two letters of her first and last name. Henrietta Lacks, a 30 year old African American woman, arrived at Johns Hopkins hospital in 1951 where she was diagnosed with cervical carcinoma; despite anti-cancer treatment, Lacks passed away later that year [1]. Meanwhile, Dr. George Gey was in the tissue research laboratory searching for a continually culturable tissue, where he had been unsuccessful until receiving biopsy samples from Ms. Lacks [2]. After realizing the power of her cells Dr. Gey began sending tissues to researchers around the country. Gey's name quickly gained recognition, however, the identification and due credit to Henrietta went unspoken for many years [1]. While doctors were unable to save Lacks, her cells have lived on to become the first "immortal" human cells to be used across the world for innovative treatments and understandings of the human cancer cell [3].

### **Overview of Quantum Dot Usage**

Many advancements have been made in the studies of cancer since the discovery of HeLa cells and specific interest has been placed on the use of quantum dot (QD) nanoparticles. First described by Ekimov et. al. as semiconductor crystals, QDs have been widely studied for their optical properties [4]. This observation of QDs is due to their unique ability to absorb photons, which results in the formation of an electron-hole pair/exciton [5]. When an electron is excited by the bulk valence band of a semiconductor, an electron-hole pair is formed; it is then confined

within the nanocrystal until recombined and colored light is emitted [6]. Additionally, changing the size of QD varies the emitted color. Due to this, QDs are becoming increasingly competitive compared to older technologies [4]. This fluorescent quality has attracted interest of many for the purpose of cancer research. The QD may act to visualize intracellular networks, marking cancer cells for diagnostic purposes, increasing radiation efficiency, targeted drug delivery, and to detect change of extracellular pH [5, 7, 8]. The applications of QDs is obviously wide spread, due to the ability to alter the composition, size, and surface charge to customize the QD to each project.

### **Customizable Properties of Quantum Dots**

One of many ways to customize QDs is by their core composition. Most commonly, variations of Cadmium (Cd), Silver (Ag), and Indium (In) have been observed. The core material can be coupled to other elements to yield varying effects on cell survival. For example, T. Zhang et. al. compared three variations of Cd QDs (Cadmium Telluride (CdTe) of 2.2 nm and 3.5 nm, and Cadmium Selenide (CdSe) of 2.2 nm) when applied *in vitro* to mouse fibroblasts. Their findings showed that the effects of QD treatment vary when changing the core and size. Treatment with 2.2 nm CdTe induced significantly higher levels of oxidative stress and percentage of apoptotic cells than the other two treatments [9]. Due to the varying toxicity that has been observed, scientists are still investigating other semiconductors with safer properties for clinical use. This hypothesis will be investigated in greater detail throughout this study and demonstrates that the choice of core composition should be carefully selected in QD treatment for the safest and most effective results.

As mentioned, changing the size of QDs changes the color of fluorescence. The relationship for this phenomenon is inverse: larger quantum dots emit lower frequencies and smaller quantum dots emit larger frequencies. The resulting color correspond to wavelengths on the color spectrum, ranging from green (495-570nm) to red (620-750nm). This property is especially important to evolving imaging technologies and has been a study of focus for many. For example, Kim et al. tested the imaging of breast cancer cells both *in vitro* and *in vivo*. To do so, Cadmium Selenium/Zinc Sulfide (CdSe/ZnS) QDs and siRNA were coupled to liposomes and viewed in breast cancer cells using fluorescent confocal imaging; their study successfully identified cellular uptake of QDs *in vitro* and shows that QDs localized to tumor tissue *in vivo*. It was importantly noted that the highest signal was detected after 8 hours of incubation [10].

It is known that far-red light travels well through human tissue, giving red-emitting QDs the potential for advancing *in vivo* imaging. Previously in pre-clinical oncology research, the use of red fluorescent protein for fluorescent tomography shows this as a non-invasive method to monitor tumor progression [11]. The same concept could therefore be applied to red fluorescent QDs targeted to tumor cells. Improvements in pre-clinical imaging of tumors will be invaluable to monitoring and treating cancer going forward.

Another use for QD imaging (specifically using blue light, wavelength 450-490nm) is exemplified by Zheng et. al. in their efforts to quantify gene expression of breast cancer tissues. The aim of this study was to compare QD-based imaging to the conventional Immunohistochemistry (IHC) technique; their results indicate that use of secondary antibodies conjugated to the QD, instead of traditional fluophores, yields better quality data, improved accuracy, and lower background disturbance than current technologies [12]. The findings of both

studies shed light on potentially clinical applications of QDs for mapping and characterizing cancer cells/tissue.

Along with improving imaging technologies, the ability to conjugate QDs to specific ligands is also noteworthy. This can be accomplished in various ways, including a biotin-streptavidin link between QD and target cell [13]. A QD-probe can also be targeted to cancer tissue via conjugation to tumor-specific antibody fragments or peptides; these advancements can detect and measure biomarkers that will go on to broaden our understanding of tumor microenvironments [14].

Besides the change in color, different sized QDs have also been seen to have varying levels of intracellular toxicity. Previously, smaller QDs decrease cell viability significantly more than larger QDs, potentially due to their ability to cross the cell membrane more easily [15]. Green CdSe/ZnS QD's (530-550nm) specifically have been seen to reduce HeLa cell viability greater than yellow (570-585nm) [16].

Another option in customizing quantum dots is changing the surface composition. The chosen surface molecule acts as a ligand for the QD and allows for selective interaction via facet charge. The three commonly studied charges are anion, neutral, or cationic and are respectively referred to as X-type, L-type, and Z-type [17]. While each charge poses its own unique advantage, it has been previously tested that carboxylic acid (R-COOH) X-type ligands are most effective in studying cellular uptake mechanisms. In their study, Zhang & Monteiro-Riviere compared dendritic cell uptake of CdS/ZnS QD coated in each type of ligand: anionic carboxylic acid (COOH), neutral polyethylene glycol (PEG), and cationic PEG-amine (NH<sub>2</sub>). Carboxylic acid coated QDs were much more easily taken up by the dendritic cells compared to positive and neutral ligands; it was theorized this is a result of carboxylic acid groups being recognized more

frequently by cellular organelles and receptors [18]. In a similar study, Lin et. al. observed aerosol pulmonary inhalation of Indium Phosphide/Zinc Sulfide QDs with each of the three surface ligands in mice. Indium, a metal in group XIII, is combined with phosphide, a  $P^{3-}$  ion, and coated with a Zinc Sulfide shell to become InP/ZnS. While all three variations of QD were successfully inhaled, the neutral coating (OH group) deposited the greatest amount of QD; in observance of lung tissue damage, only the Z-type coating (NH<sub>2</sub> group) showed signs of causing alveolar septal hyperemia [19]. Collectively, it is important to take surface charge into account when selecting QDs for different exposure routes and test organisms. In the present study understanding the mechanism and result of cellular uptake is desired, leading to X-type COOH surface coated QD to be selected for observation.

### **Resulting Toxicity from Quantum Dot Treatment**

As discussed, QDs have raised alarm for inducing cytotoxicity within contacted cells. Among these potentially harmful QDs, those composed of cadmium (Cd) cores, such as CdSe, CdTe, and Cadmium Sulfide (CdS), are the most commonly studied and have become well known for reducing cell viability. Cadmium is a transition metal, located in group XII of the periodic table, and is known for being a human carcinogen. The toxicity of this core has been linked to a result of  $Cd^{2+}$  ions that damage the cells it comes into contact with [20]. Studying the effects of Cd specifically within HeLa cells, Hens et.al. found CdS/ZnS QD that emit green light reduced cell viability more extensively than the same QD emitting yellow fluorescence, further suggesting different sizes of QD can be more harmful than others [16]. Another example of cellular damage from Cd QD exposure is shown by Roberts et. al. in which they show lung inflammation and injury after pulmonary exposure in mice; measurable damage peaked 7 days

after exposure. The authors used fluorescent imaging to hypothesize that the QD is destabilized by the lung, resulting in removal of the stabilizing ZnS shell and subsequent release of free Cd that resulted in tissue inflammation/damage [21]. This trend was observed similarly *in vivo* by M. Wang et. al., where Cd QD induced tissue damage was also most significant after 7-14 days. The authors suggest the damage can be reversible in time, as damage was reduced at day 28 post-treatment [22].

Solutions to QD toxicity are currently being tested. Shells of ZnS have been added around the Cd QD core and have shown to slightly reduce cytotoxicity and highly improve biocompatibility [23]. It is hypothesized that the shell prevents Cd<sup>2+</sup> ions from leaking out of the core and into the affected cell. Observed by Williams et. al., membrane disruption and stability vary with the number of shell monolayers, as well as the core structure [24]. Horstmann et. al. explains that the relationship between the core and shell possibly affects the stability of the QD. Therefore, the number of layers and core composition should be adjusted for maximum strength and functionality [25].

### **InP Alternative to Cd Quantum Dot**

As cytotoxicity of QDs with Cd core is a rising concern within the field, alternative cores are being investigated. Indium Phosphide/Zinc Sulfide (InP/ZnS), prepared in the same manner as Cd/ZnS QDs, was introduced by scientists as a safer option to Cd QDs [20]. Being an under-developed field, there is not enough data to confirm whether InP QD is more/less toxic compared to Cd. So far, studies have found varying conclusions. For example, Ayupova et al. found, in macrophage-like cells, InP/ZnS treatment yielded significantly lower cytotoxicity than Cd QD treatment based on viability and reactive oxygen species (ROS) observations [26]. In lung-



derived cell lines, InP/ZnS treatment increased apoptosis and ROS generation at high concentrations [20]. The authors warn that InP still yields cytotoxicity and note that concentration and surface composition should be carefully considered in future applications. Understanding the inflammatory response to InP/ZnS treatment is also important to determining their safety in clinical settings; shown by S. Chen et al. IL-6 (an inflammatory cytokine) was stimulated upon treatment, resulting in acute inflammation and oxidative stress within macrophages [27]. Overall, detailed properties should be adjusted when making InP/ZnS QDs so that the most effective and safe combination can be used going forward.

The cytotoxic effects of QD treatment have scientists concerned for their safety in mammalian cells. However, what if it were possible to harness the toxicity of QD for good? With a better understanding of the mechanisms of QDs, they could be useful tools in anti-cancer therapies. Specifically, they have been speculated for use of targeted drug delivery and photodynamic therapies [28]. The trick will be to design a QD able to penetrate and destroy cancerous cells, while leaving regular tissue unharmed. As current literature has yet to conclude whether this is possible, the present study aims to make progress in understanding if InP QD could be the right material for the job. With expanded research and knowledge about this alternative QD, it can be determined if InP is a safe, yet effective, treatment to use against cancerous mammalian cells.

### **Problem Statement and Hypothesis**

In this study, we aimed to observe and expand knowledge on the effects of InP/ZnS QD when introduced to HeLa cells. To investigate the claim that InP is a less toxic alternative to Cd QD, we hypothesized InP/ZnS to not decrease HeLa cell viability. To test this, we used XTT cell

viability, reactive oxygen species, and apoptosis assays. We also compared the transcriptome of treated HeLa cells to the human genome. Our findings led us to map physiological pathways that explain how QDs can interact with the cell. Prior research of InP QDs is limited, however, the present study's findings provide promising insight to the use of QDs as an effective anti-cancer therapy.

## MATERIALS AND METHODS

### InP/ZnS Quantum Dots

InP/ZnS QDs conjugated with carboxylic acid ligands were obtained from NN-Labs (Fayetteville, AR, USA) and suspended in water (1 mg/mL). The QDs are capped with ZnS shell surrounding the InP core for stability and to improve biocompatibility. Green InP/ZnS QDs emit at 530 nm +/- 15 nm and are 3.7 +/- 0.5 nm in diameter.

A chemical and physical properties analysis of the commercially purchased QDs was conducted using scanning transmission electron microscopy (STEM), energy dispersive x-ray spectroscopy (EDAX), ultraviolet-visible (UV–VIS) spectroscopy, and dynamic light scattering (DLS). The stock (INPW530) QD material was diluted to a concentration of 100 µg/mL and was used for each proceeding study.

A JEOL 7900F scanning electron microscope (SEM) with a scanning transmission electron microscopy (STEM) detector was used to image the QDs for qualitative dimensional analysis. The diluted QD dispersion was drop cast onto holy carbon film TEM grids and allowed to air dry in a desiccator box prior to imaging. Elemental composition of the InP/ZnS QDs was measured using a Bruker Quantax energy dispersive x-ray spectrometer (EDAX) attached to the SEM. A thick film of the InP/ZnS QDs was deposited using a drop cast method onto a silicon substrate prior to analysis.

Dynamic light scattering (DLS) technique was used to characterize the hydrodynamic size of the InP/ZnS QDs which were diluted in water and cell media. The diluted samples were tested with a Malvern Panalytical Zetasizer® Ultra with laser wavelength of 632 nm and scattering

angle of 173°. The UV-Vis absorption spectrum was recorded with a Shimadzu UV3600 UV-Vis-NIR Spectrometer with scan range of 200 nm to 800 nm and a step size of 0.5 nm.

## **Cell Culture**

We chose two cell types for the present study: HeLa-S3 cells (authenticated by Genetica Labs of Burlington, NC) and mouse fibroblast. The protocols for both cell lines were the same. First, cells from a -80 °C freezer thawed to 37 °C. To collect a pellet, the thawed cells are immersed in Dulbecco's Modified Eagle Medium (DMEM) prepared with 10% penicillin/streptomycin antibiotics and 10% Fetal Bovine Serum (FBS). Removal of the supernatant after centrifugation (440g for 10 min) reveals a cell pellet that is then resuspended in 13 mL of prepared DMEM+PS+FBS. Plated cells then grew until confluent in an incubator maintaining 37 °C with an atmosphere of 5% CO<sub>2</sub>/95% air; changing the media every few days allowed for maintenance of cell growth.

## **XTT Viability Assay**

Both HeLa-S3 and mouse fibroblast cells separately underwent XTT viability assay to compare effects of InP/ZnS QDs on cancerous and non-cancerous mammalian cells. Biotium manufacturer protocols led the experimental design development. After seeding (7,500 cells/well) into a flat-bottom, 96 well plate, the cells incubated at 37°C for 24 hours. On the second day, fresh DMEM replaced the previous media (100 µL/well). Designated treatment wells were given 20 µL of InP/ZnS and serially diluted by a factor of five to give a concentration range of 0.13 µg/mL to 167 µg/mL. Additional wells served as a positive control and contained Dimethylsulfoxide (DMSO) at three different concentrations: 5, 10, and 15 %. The plates then

incubated for another 24 hours. The following day, an XTT solution was prepared in 1:200 ratio of XTT solution and XTT Activation Reagent (PMS) respectively. The solution applied to each well of the plate (25  $\mu$ L/well) and remained for 7 hours at 37 °C. Formazan dye formed in the wells to allow for quantification of viable cells using BioTek ELx880 Absorbance Microplate Reader (absorbance measured at wavelength 450 nm and 630nm). Subtracting the absorbance value at 450nm (A450) by the absorbance at 630nm (A630) accurately measures the amount of dye, and level of viable cells, after 7 hours. A total of two trials of this experiment were completed; in each trial, each sample was done in triplicate experimental replicates.

### **Calculation of IC<sub>50</sub> Value**

The AAT Bioquest website (<https://www.aatbio.com/tools/ic50-calculator>) calculated the concentration at which 50% of cell growth was inhibited (IC<sub>50</sub>). Data from XXT cell viability assay uploaded to the equation and calculated IC<sub>50</sub> to be 69  $\mu$ g/mL. The equation used can be seen in Equation 1. The calculated IC<sub>50</sub> value further applied to all consecutive experiments as the main treatment concentration.

### **Reactive Oxygen Species Assay**

Reactive oxygen species (ROS) assay took place over a three-day period. To begin, fresh HeLa cells seeded into two separate 24-well plates (50,000 cells/well) and incubated for 24 hours. Following this, InP/ZnS QDs then applied equally to both plates in two different concentrations: 69  $\mu$ g/mL and 167  $\mu$ g/mL. The plates incubated for another 24 hours. On the third day, the cells needed to be detached from the well to be available for harvest. After removal of DMEM, 500  $\mu$ L of 1xPhosphate-buffered saline (PBS) washed each well two times. The

1xPBS was removed so that 250  $\mu$ L of trypsin + ethylenediaminetetraacetic acid (EDTA) could submerge each well for 15 minutes to detach cells. DMEM (250  $\mu$ L/well) adds to the trypsin in each plate well after incubation and each detached sample then transferred to 2 mL microcentrifuge tubes. These centrifuge for 10 minutes at a speed of 400 x g. During centrifugation, 0.5 mg of indicator and 1 mL DMSO mixed to create two ROS indicator solutions (Dihydroethidium (DHE) and Dihydrorhodamine 123(DHR)). The samples obtained from one plate receive DHE solution and the other DHR. Removal of the supernatant in each centrifuged tube left a pellet to be resuspended in 10  $\mu$ L of the corresponding indicator and 990  $\mu$ L of 1xPBS. Foil protected the samples from light exposure and covered them during a 30-minute incubation at 37 °C before being analyzed by Life Technologies Attune NxT Flow Cytometer. Samples dyed with DHE measure at 518/606 nm and those with DHR at 507/536nm.

### **Apoptosis Assay**

Before beginning the apoptosis assay, 10X Annexin V Binding buffer was prepared by mixing concentrations of 0.1M HEPES, 1.5M sodium chloride (NaCl), 25mM calcium chloride ( $\text{CaCl}_2$ ), and molecular grade sterile water. For experimental use, 18 mL of 1xPBS diluted 2 mL of the 10X Annexin V Binding buffer to be a 1x solution. To initiate the experiment, HeLa cells seeded at 50,000 cells/well into a 24 well plate. After incubating for 24 hours, treatment applied at two different concentrations of InP/ZnS QDs: 69  $\mu$ g/mL and 167  $\mu$ g/mL. On the third day, 1xPBS washed each well two times and non-EDTA trypsin (250  $\mu$ L/well) detached the cells from the bottom of the well. Following incubating for 20 minutes, 250  $\mu$ L of DMEM adds to mix with the trypsin. The samples, then transferred to microcentrifuge tubes, centrifuged for 10 minutes at 2000 x g and the supernatant was removed. The remaining pellets of untreated and

negative control samples resuspended in 500  $\mu\text{L}$  1xPBS. Positive controls and treated samples resuspended in 100  $\mu\text{L}$  1x Annexin V Binding buffer, 5  $\mu\text{L}$  Annexin V-APC (measuring early apoptosis), and 5  $\mu\text{L}$  propidium iodide (PI) (measuring late apoptosis). Once incubating in the dark for 30 minutes, another 400  $\mu\text{L}$  of 1x binding buffer was added to the samples. Life Technologies Attune Nxt Flow cytometer then measured each sample based on the excitation properties of the dyes. Annexin V-APC emits at 650 nm with a red laser, and PI emits at 617 nm with a blue laser.

### **Total RNA Extraction and cDNA Conversion**

HeLa cells treated with 100  $\mu\text{g}/\text{mL}$  InP/ZnS underwent a total RNA extraction in order to analyze changes to the cell transcriptome. To begin, 750,000 cells seeded into each well of a 6 well plate and incubated for 24 hours. Using Invitrogen TRIzol protocols, total RNA was extracted and resuspended in 30  $\mu\text{L}$  of nuclease-free water. Qubit 3.0 Fluorometer at 280 nm OD measured the concentration of RNA in each sample. TruSeq<sup>®</sup> Stranded mRNA LT Sample Preparation Kit (Illumina, San Diego, CA) isolated mRNA. One ng of mRNA isolate synthesized 6 cDNA samples, 3 non-treated and 3 InP/ZnS treated, with Verso Reverse Transcriptase kit (using Thermo Scientific protocol). A different adaptor ligated each sample and amplified it 15 times in T100<sup>TM</sup> Thermal Cycler (BIO-RAD). The resulting cDNA served for subsequent transcriptome analysis.

### **RNAseq Transcriptome Analysis**

To determine significantly altered genes, the University of Kansas Medical Genome Centre sequenced cDNA samples of treated and non-treated cells. Illumina Hiseq 2500 sequencing

system processed cDNA samples with 100 nucleotide sequences of each end. The data then uploaded to the Basepair Tech website ([www.basepairtech.com](http://www.basepairtech.com)). From there, the website conducted pipeline RNA-seq and total expression count on the sequences. Results were aligned with the human reference genome (hg19) via differential expression (DESeq2) to produce a list of effected genes. The list of genes transferred to GOrilla, where Microsoft Excel grouped Gene Ontology (GO) terms by significance and function.

### **Statistical Analysis**

Each analysis was repeated multiple times and the most consistent trial was reported. Within each experiment, every sample had 3 experimental replicates that were then averaged during analysis. GraphPad Prism 8.0 statistically analyzed data of all experiments. One-Way ANOVA analysis and Dunnett's multiple comparisons visualized any variance among control and treatment groups. Statistically significant data is represented on graphs as \*  $p < 0.05$ , \*\*  $p < 0.01$ , \*\*\*  $p < 0.001$ , \*\*\*\*  $p < 0.0001$ .



## RESULTS

### Chemophysical Properties of Green InP/ZnS

A JEOL 7900F scanning electron microscope (SEM) with a scanning transmission electron microscopy (STEM) detector was used to image the individual QDs. The sample INPW530 (InP/ZnS – 530nm) was diluted to a concentration of 0.1 mg/mL and subsequently drop cast onto holey carbon film TEM grids and allowed to air dry in a desiccator box. Figure 1 shows the STEM images which approximates the InP/ZnS QD particle sizes in agreement with that of the data sheet values (3.7 – 5.2 nm).

Elemental composition of the InP/ZnS QDs was measured using a Bruker Quantax energy dispersive x-ray spectrometer (EDAX). A thick film of each of the InP/ZnS QDs (530nm) was deposited onto silicon substrates. The spectra of QD sample is provided in Figure 2, which verifies the InP/ZnS composition.

Dynamic light scattering (DLS) technique was used to characterize the hydrodynamic size of InP/ZnS quantum dots dispersion in aqueous solution. QDs samples at 0.1mg/mL were tested by Malvern Panalytical Zetasizer® Ultra with laser wavelength of 632nm and scattering angle of 173°. DLS results (Figure 3) showed a monodisperse peak with hydrodynamic diameter of 72.3nm InP/ZnS. The results indicate that there might be formation of ligands shells (carboxylic acid ligands) and also possible aggregations when the QDs were dispersed in aqueous solution.

UV-Vis absorption spectrum was recorded by a Shimadzu UV3600 UV-Vis-NIR Spectrometer with scan range of 200 to 800nm and step size of 0.5nm. A sample was diluted to 0.1mg/ml by DI water. InP/ZnS showed no absorption at or above wavelengths of 650nm (Figure 4a). The first absorption peak for InP/ZnS were around 470nm (Figure 4b).

The thick film of InP/ZnS QDs that were deposited onto silicon substrates were excited using a UV source at 365nm. Figure 5 shows the excitation at 530nm (Green).

### **Effect on Cell Viability When Treated with InP/ZnS QD**

To examine the toxicity of InP/ZnS QD when treated to HeLa cells, an XTT assay was performed. Cells were treated with concentrations ranging from 0.13  $\mu\text{g/mL}$  to 167  $\mu\text{g/mL}$ , serially diluted by a factor of 6x for 24 hours (Figure 6A). Then, XTT assay dye was added. When cells are alive, mitochondrial enzymes reduce the XTT dye to form an orange color. The generated color is measured by absorbance and is equivalent to the number of viable cells (higher absorbance equaling higher cell viability). After 7 hours of incubation with XTT dye, HeLa cell viability was reduced to approximately 68% when treated with 167  $\mu\text{g/mL}$  InP/ZnS compared to the non-treated control. At this concentration, samples averaged an absorbance level of 0.23, which was deemed statistically significant by One-way ANOVA test (Figure 6A). All other concentrations, including the control, averaged absorption levels between 0.31-0.33. Based on these results, 167  $\mu\text{g/mL}$  was used as the minimum inhibition concentration for further experiments. DMSO (concentration ranging from 5%-20%) was used as a positive control and showed lower absorbance levels compared to the non-treated control (NTC).

Mice fibroblast cells were tested in the same manner to observe effect of InP/ZnS treatment in non-cancerous tissue. Interestingly, there was an increase in cell viability compared to the NTC in all concentration levels (Figure 6B). Treatment concentrations ranged from 0.13  $\mu\text{g/mL}$  to 167  $\mu\text{g/mL}$ ; at the highest concentration, absorbance increased to 0.36 (compared to the control of 0.19). This finding is highly valuable in the potential of InP/ZnS QDs in cancer treatment. The ability of the chemical to decrease viable cancer cells while leaving non-

cancerous tissue unharmed is very desirable. Expanding the studies on InP/ZnS QD treated fibroblast tissue will improve the viability of the result and plausibility of these QDs as anti-cancer therapy.

### **Increased Production of Superoxide and Peroxynitrite Radicals in InP/ZnS Presence**

The production of Reactive Oxygen Species in the form of free radicals is a known reaction of cellular metabolism that, when increased, plays a large role in disturbing the survival of the cell in stressful environments. ROS are produced in several organelles including the mitochondria. While normal levels of mitochondrial ROS are managed by antioxidant mechanisms, oxidative stress caused by elevated ROS results in mitochondrial dysfunction and activation of cell death pathways [29, 30]. We tested for ROS production of two molecules in cells treated with 69  $\mu\text{g/mL}$  and 167  $\mu\text{g/mL}$  InP/ZnS. Samples were dyed with dihydroethidium (DHE) to measure cells producing superoxide radicals and with dihydrorhodamine (DHR) to measure those producing peroxynitrite. If cells exhibit fluorescence at a peak excitation wavelength of 518nm due to DHE treatment (or 530nm, due to DHR treatment), then they would be positive for producing superoxide radicals (or peroxynitrite). As each sample was repeated in triplicate, the average for each concentration level was compared via bar graph (Figure 7A&B). Fluorescent peaks of each sample were observed with flow cytometry and gates were used to measure percentage of cells producing ROS (Figure 7C-H). When measuring the entirety of present cells, those treated with InP/ZnS exhibited fewer fluorescent positive cells than in the dyed, non-treated control – revealing a significant decrease in superoxide radical production compared to the dyed, NTC (Dyed control averaging 79.18% ROS production). Both concentrations of InP/ZnS

treatment yielded similar percentages of change; 69  $\mu\text{g/mL}$  InP/ZnS averaged 56.34% ROS positive cells and 167  $\mu\text{g/mL}$  InP/ZnS averaged 51.89% (Figure 7A). Based on the use of the DHR dye, InP/ZnS treated cells exhibited an increased production of peroxynitrite (averaging 57.85% ROS positive cells) as compared to the NTC (Figure 7B). Again, the increased amount of peroxynitrite positive cells were similar at both concentrations of treatment. Samples treated with 69  $\mu\text{g/mL}$  InP/ZnS averaged 79.28% ROS production, while those treated with 167  $\mu\text{g/mL}$  InP/ZnS averaged 78.13%.

Continuing the analysis, median fluorescent intensity (MFI) was also measured to calculate an accurate level of ROS production only in living, viable cells. MFI also shows intensity/degree of ROS production. MFI measurements revealed an increase in both superoxide and peroxynitrite positive cells compared to the NTC as well as a greater intensity of ROS (Table 1). As the original measurements (Figure 7) included unviable cells, it is likely the decreased levels of superoxide is due to a significant amount of cells already being unviable and incapable of producing ROS. By only observing viable cells with MFI, the measure of ROS producing cells is more accurate to analyzing the change compared to NTC. Collectively, I hypothesize the QD treatment to significantly increase production of both superoxide and peroxynitrite ROS molecules. The increase could also be causing oxidative damage and induction of cell death, which would henceforth explain the large amount of unviable cells disrupting the appearance of the original measurements. As superoxide radicals are formed in the mitochondria, they can collide with nitric oxide to form peroxynitrite; this causes cellular dysfunction and cell death [31]. This pathway could help further explain the observed increase in peroxynitrite production, as more superoxide (a reactant) became available to make-up the product.

## Increased Late Apoptosis with InP/ZnS Treatment

Increased levels of ROS induce stress upon affected cells by causing damage to multiple intracellular components, which often leads to induction of apoptosis [32]. Understanding how apoptotic-like programmed cell death occurs is important to elucidating tumor suppression mechanisms and advancements in anti-cancer drugs [33]. We tested for an induction of apoptosis in cells treated with 69  $\mu\text{g/mL}$  and 167  $\mu\text{g/mL}$  of InP/ZnS QDs (Figure 8A-E). Our results were divided into early and late apoptosis and observed with gated quadrants using flow cytometry (Figure 8C-E). Early apoptosis involves the activation of multiple signal cascades and can be measured by the presence of phosphatidylserine (PS) in the plasma membrane (detected with annexin V); late apoptosis represents the fragmentation of DNA and the loss of cell membrane integrity [34]. In both concentrations of treatment groups, the amount of cells undergoing apoptosis was decreased in the early phase and increased in the late phase. The dyed control for early stage (Figure 8A&C) averaged 27.7% of cells undergoing apoptosis, while that for late apoptosis (Figure 8B&D) averaged 0.69%. There was not a significant difference in the two concentrations of treatment, indicating the  $\text{IC}_{50}$  (69  $\mu\text{g/mL}$  InP/ZnS) is a sufficient dose to change levels of apoptosis. At 69  $\mu\text{g/mL}$  InP/ZnS, early apoptosis averaged 15.24%, a 45% decrease from the control group. At 167  $\mu\text{g/mL}$  InP/ZnS, samples averaged 19.48% early apoptosis- a 29.7% difference decrease compared to NTC. As for late apoptosis, 69  $\mu\text{g/mL}$  InP/ZnS averaged 31.28%, nearly 4417% increase from the control group. 167  $\mu\text{g/mL}$  InP/ZnS averaged 23.67%- a 3317%.

## Altered Genome with InP/ZnS Treatment

RNA-seq results aligned with the human reference genome showed 16.4k genes differentially expressed. The data were filtered for  $p$ -value  $< 0.05$ , which resulted in 620 downregulated genes and 1129 upregulated genes. The 1129 upregulated genes were sorted by function and yielded strong activation of developmental processes (such as cell differentiation, tissue and nervous system development, and morphogenesis) and signal transduction (including stimulus responses, G protein-coupled receptor signaling, and inflammatory responses) (Figure 9A). Specific genes involved with developmental processes include *LGALS9*, *ZSWIM4*, and *IFITM1*; those involved with signal transduction are *RFNG*, *MEIS3*, and *SYN1*. The same process was performed with the 620 downregulated genes. This yielded major disruption (over 300 altered genes) of metabolic processes and biosynthetic process regulations (Figure 9B). Those involved with metabolic processes included *NCBP2*, *DPM1*, and *BCAS2*; biosynthetic process genes included *PSMC6*, *PSMD12*, and *PSMD14*. A second filter was then applied to select genes with a log2 fold change greater than 1. This resulted in 69 downregulated and 408 upregulated with  $p < 0.05$  and log2 fold change  $> 1$  (Figure 9C-D). The functions of the highly downregulated genes were investigated to show significant disruption to cell growth regulation, protein quality controls, and mitochondrial function. Notable genes in this category are *PDK4*, *ID2*, *SRRM4*, and *MMP13*. Highly upregulated genes commonly coded for transmembrane proteins to alter proliferation, apoptosis, cellular transport, and organization. Significant genes for upregulation include *TIMP1*, *ZSWIM4*, and *LGALS9*.

## DISCUSSION

QDs have potential to advance medical techniques such as molecular imaging and anti-cancer treatment. InP/ZnS QDs have been proposed as a safer alternative to Cd based QDs but have not been previously investigated enough to understand how they alter cellular homeostasis, function, and the transcriptome. This study aims to fill the gap in this knowledge. Through a series of experiments, we suggest the impact of InP/ZnS QDs interacting with HeLa cells and the results they have. We found increased levels of oxidative stress and apoptosis, supporting previously stated hypotheses positing that toxicity is associated with QD treatment. Investigation of the transcriptome via RNA-seq offers evidence of transcriptome alteration and are explained with diagrams mapping genetic alteration throughout the cell. Our findings are significant for understanding more about the effects of InP/ZnS QD exposure, but further investigation is required to understand if they are a viable technology for medical treatment.

### **Changes to HeLa Cell Viability, ROS, and Apoptosis Levels with InP/ZnS Treatment**

When observing cell viability after 24 hours of InP/ZnS treatment, 167  $\mu\text{g/mL}$  InP/ZnS significantly decreased cell survival by 32%. Among the current data, the consensus on InP/ZnS effect on cell viability seems to vary by cell type and length of treatment. For example, Chen T et. al. observed varying decrease in viability after 24 and 48 hours of treatment to human lung cancer cell (HCC-15) and alveolar type II epithelial cell (RLE-6TN) (treatment concentrations ranging 80-160  $\mu\text{g/mL}$  InP/ZnS). Treatment of REL-6TN cells at 160  $\mu\text{g/mL}$  resulted in 80% viability after 24 hours, which reduced to 40% viability after 48 hours [20]. In a similar study, treatment for 24 hours at 80  $\mu\text{g/mL}$  and below did not significantly decrease cell viability in bone

marrow-derived macrophages of mice [27]. Collectively, these findings suggest that HeLa cells are susceptible to InP/ZnS related damage and are shown in the present study as reduced in viability by 32% compared to NTC. The degree of susceptibility seems to vary across cell lines, and impact greatens with treatment dosage. Further investigation with varying treatment concentrations and length of exposure could aid in better understanding this comparison.

The decrease in HeLa viability may be supported by RNAseq results as well. Presently, ATF3 is slightly upregulated by InP/ZnS QD treatment (0.23 fold change). Fan et. al. observed the ATF3 response to DNA damage in HeLa cells, finding the overexpression to potentially slow the cell cycle progression [35]. The use of InP/ZnS QD treatment to prevent cancer cell growth via genetic alteration could be an important of HeLa studies going forward.

The influences of QDs on ROS production, specifically InP/ZnS QDs, has been previously reported [36–39]. ROS consist of many metabolites that induce stress within the cell including superoxide, hydrogen peroxide ( $H_2O_2$ ) and peroxynitrite. Each of the metabolites mentioned are measured with a different fluorescent probe: DHE, DCFH-DA, and DHR, respectively. Additionally, superoxide can merge with nitric oxide to form peroxynitrite, or superoxide dismutase to make  $H_2O_2$ . Focusing on DHE and DHR, we observed cellular production of superoxide radicals and peroxynitrite levels increased when analyzing only viable cells. Current literature is in agreeance with our finding as QDs have been seen to induce ROS production across many different cell types. For example, Ayupova et. al. also reports increased production of superoxide radials in RAW 264.7 murine “macrophage-like” cells after InP/ZnS QD treatment (1 mg/mL); they also observed a decrease in the anti-oxidant GSH which would allow for cellular oxidative stress to progress [26]. T. Chen et. al. reported significant increases in ROS (in form of  $H_2O_2$ ) in two different lung-derived cell lines which they pose to explain the observed



cytotoxicity with InP/ZnS QD treatment [20]. Collectively, QDs seem to be disrupting mitochondrial function by surging an increase in ROS production; this is likely causing oxidative stress and induction of cell death.

Increased oxidative stress by ROS has been linked to inducing apoptosis as well. Presently, we observed a significant increase of late apoptosis. Levels of early apoptotic cells were decreased, likely because most of the active cells had already shifted towards the late stage of cell death. Cells positive for early apoptosis were observed in the dyed control as well (Figure 8A); it is possible this is a result of drying during culturing or damage during plate detachment via trypsin.

T. Chen et. al. also observed increased levels of ROS and apoptosis in lung derived cell lines. This is consistent with an observed increase of late apoptosis in our study, however T. Chen et. al. reported significant increase of apoptosis at a much lower concentration of InP/ZnS QDs (20  $\mu\text{g}/\text{mL}$  compared to 69  $\mu\text{g}/\text{mL}$  and 167  $\mu\text{g}/\text{mL}$ ) [20]. At 28  $\mu\text{g}/\text{mL}$  InP/ZnS, we did not find cell viability to be significantly changed (Figure 6); variation in InP/ZnS toxicity is documented between cell types and presents an area of study to be expanded in the future.

### **Upregulated Gene Processes Increase ROS Production and Induce Apoptosis**

After observing increases of ROS and apoptotic induction, we turned to RNAseq data for upregulated genetic sequences that could support these results. QDs are known to cause ROS increase by activation of the caspase-1 by assembly of the NLRP3 inflammasome [40].

Presently, *CASP1* is upregulated by 0.63 fold change and could help explain the increased ROS seen with InP/ZnS treatment. Also in HeLa cells, *C. trachomatis* has been shown to increase

ROS and induce CASP1 activation [41]. Collectively with previous data, we hypothesize the upregulation of CASP1 to support the increased ROS seen in Fig 7.

Supporting our findings of increased late apoptosis (Figure 8), another gene that was upregulated, *LGALS9*, has been shown to play a role in apoptosis (Figure 10A). This gene is responsible for suppressing T-cell proliferation, inducing T-cell apoptosis, and associated with angiogenesis and cytokine signaling; it has also been studied specifically for anti-cancer activity [42]. Immune function was observed by Holderried et. al. by investigation of T cell-mediated tumor evasion. Galactin-9, a ligand made by *LGALS9*, was upregulated in colorectal tumors and hypothesized to be a therapeutic target for immune-mediated anti-cancer therapies by inducing apoptosis [43].

Increased *ZC3H12A* expression also point to apoptosis. *ZC3H12A*, a transcription factor, is proposed to induce apoptotic gene expression and regulate inflammation/stress responses. Studied in colorectal cancer patients, T. Chen et al. found lower expression levels of *ZC3H12A* are seen in more aggressive tumor cells; thus, increasing *ZC3H12A* expression might be effective in making cancerous tissue less aggressive [44]. Going forward, targeted therapies could explore use of this gene for inducing tumor cell death.

We also report up regulation of *ZSWIM4*, potentially involved in chromatic organization. We suspect disruption of this gene could lead to disruption of *ZC3H12A* as well (Figure 10A). Our results suggest InP/ZnS QDs induces stress on the cell, which increases *ZSWIM4* and *ZC3H12A* expression and induces apoptosis.

Along with *ZC3H12A*, *LIF* and *LGALS9* upregulation has been associated with collateral damage via the immune system. Leukemia inhibitory factor (*LIF*) is a member of interleukin 6 pro-inflammatory cytokine family and is responsible for inhibiting cell growth and

differentiation. In their study with elephant cells, Vazquez et. al. report upregulation of *LIF* results in DNA damage and leads to apoptosis; the authors propose this to be linked to evolution of cancer resistance in organisms with long life spans [45]. Immune function of *LGALS9* was observed by Holderried et. al. by investigation of T cell-mediated tumor evasion. Galactin-9, a ligand made by *LGALS9*, was upregulated in colorectal tumors and hypothesized to be a therapeutic target for immune-mediated anti-cancer therapies [43]. Collectively, we suggest cellular stress could activate the immune system in the presence of InP/ZnS QDs and induce apoptosis in tumor cells (Figure 10A).

In analyzing up regulated genes from InP/ZnS QDs treatment, genes controlling metastatic inhibition and increased cell aggregation were overexpressed. Specifically *ITGAI*, an integrin protein involved in cell adhesion and surface signaling, has been linked to both apoptosis and cell aggregation. Saftencu et al. observed papillary thyroid cancer RNA, finding *ITGAI0*, and other biological adhesion genes, as having prognostic impact by linking increased gene expression to patient survival [46]. Additionally, *TIMP1* is an inhibitor of matrix metalloproteinase (MMP) and involved in apoptotic pathways of synovial fibroblasts. Prior studies of Dumortier et al. have shown *MMP13* role in breast tumorigenesis. In their findings, the inhibition of MMP was linked to regulating cell migration and apoptosis [47]. Thus along with increased induction of apoptosis, we suggest the genetic control of metastasis as a future study point in the potential of InP/ZnS as anti-cancer therapy.

### **Downregulated Processes Also Prevent Tumor Growth Via Oxidative Stress**

Genetic inhibitions also support our findings of oxidative stress and elevated apoptosis. A member of the pyruvate dehydrogenase kinase (PDK) family, PDKs function to regulate

carbohydrate metabolism in mammals by catalyzing oxidative decarboxylation of pyruvate [48]. The presence of PDK4 expression has been said to improve mediation of mitochondrial ROS; PDK4 deficiency is also suggested to cause mitochondrial-mediated apoptosis as a result of ROS oxidative stress [49]. RNAseq revealed decreased *PDK4* expression (-1.3 fold change) (Figure 10B). We hypothesize this down regulation to support our findings of ROS generation and subsequent apoptotic induction in HeLa cells treated with InP/ZnS QDs.

Expression of HIGD1A is shown to interact with the mitochondrial electron transport chain to control ROS production [50]. Currently, we see a decrease in HIGD1A expression (-0.85 fold change). Its reduction has previously been linked to breast cancer tumor recurrence [51]. It is noteworthy that the down regulation seen in our RNAseq is likely because we are also observing a cancer cell. However, it would be interesting to observe this gene more closely in HeLa cells; possibly targeting the expression in tumor cells could act to control the ROS production commonly induced by QD treatment. We suggest HIGD1A as a focus for gene-focused cancer therapies in the future.

Earlier, the up regulation of *LGALS9* and *ZC3H12A* was linked to apoptosis. Similarly, down regulation of *ID2* could provide another mechanism of inhibiting tumor cell proliferation. *ID2* (Figure 10B) has been investigated as an important activator in tumor progression in glioma and breast tissues [52–54]. We therefore suggest gene targeting as topic of further investigation for genetic prevention of tumor growth.

Alternative splicing in mRNA creates recombinant and diverse proteomes within a cell and increases tumor aggressiveness; in previous studies, a common regulator and potential therapeutic target of this process is *SRRM4* [55, 56]. Presently, *SRRM4* levels were inhibited by InP/ZnS QD treatment, possibly showing an ability to alter the *SRRM4* communication pathway

(Figure 10B). Signaling mechanisms of *SRRM4* have been proposed to show an ability to drive tumor progression, aiding in future development of resistance therapies [57]. We suggest *SRRM4* as another future interest for genetic anti-cancer therapies involving InP/ZnS QD treatment.

*UMODL1* was also down regulated (Figure 10B). This gene is associated with immune and female reproductive systems and peptidase inhibition, however data explaining its role in cancer is sparse. Available studies have linked *UMODL1* to lung cancer metastasis [58] and ovarian degradation when upregulated [59]. Originally, we had suspected a decrease in *UMODL1* expression to show tissue degradation by excess peptide breakdown. However, this is contradicting to the findings of W. Wang in which they link ovarian degradation to an increase of *UMODL1* expression [59]. While ovarian and cervical tissues are closely related in the body, it is important to note that gene response can vary among organ tissues. Linkage to excessive tissue breakdown pose a negative side effect to InP/ZnS QD treatment in HeLa cells, however an expansion in testing is necessary to further understand *UMODL1*'s influence in cervical cancer.

We mentioned above that *TIMP1* expression inhibits that of MMPs. We support this with our RNAseq results yielding increased *TIMP1* and decreased *MMP13* expressions (Figure 10B). *MMP13* is an MMP transcription factor in the collagenase family. We suspect upregulation of *TIMP1* to have a role in this. *MMP13* has been found to be overexpressed in breast cancer tissues and contributes to the breakdown of ECM collagen to promote metastasis [47, 60]. Stemming from this, we suggest future investigation on the inhibition of MMPs to evaluate it as a potential gene target for preventing tumor metastasis via inhibition of ECM degradation.

Our findings support InP/ZnS treatment to have potential in controlling tumor growth by suppressing proliferation and metastasis. The observed decrease in cell viability contrasts from

the original hypothesis, as InP was expected to be safer for cellular treatment. Because viability is inhibited, we suggest InP/ZnS QDs to have potential for anti-cancer treatment in mammals. Before this will be possible, further assessment and understanding is required. We acknowledge limitations within this study and suggest subsequent experiments with HeLa cells and InP/ZnS QDs before recommending them to be a safe, reliable option for medical applications and beyond. While the current study shows a broad range of treatment concentrations, it lacks small intervals between each. The large gaps in treatment concentrations limit data that would pinpoint the concentration of InP/ZnS that significantly decreases cell viability. Future studies may focus on smaller ranges of treatment to understand this point further. The comparison of these results to Cd QD treated HeLa cells will also be beneficial to determining if InP is less toxic when compared to Cd. With diversified studies, better understanding of QD inflicted toxicity will progress the potential contribution to clinical treatment and technology.

## CONCLUSION AND FUTURE STUDIES

The toxicity of QDs has raised concerns against their uses in medical and scientific technology. Being proposed as a safer alternative to Cd based QDs, InP QD were studied for their effects on viability, reactive oxygen species, apoptosis, and the transcriptome of HeLa cells. Contrary to the original hypothesis, InP/ZnS exposed cell viability was depleted, while ROS and apoptosis levels were elevated (69 and 167  $\mu\text{g/mL}$ ). The transcriptome had many alterations in presence of the InP/ZnS QD that can be linked to preventing proliferation and metastasis, as well as inducing apoptosis and cytokine release. Thus, our data does not support the claim InP/ZnS QDs is necessarily safer than Cd QDs. However, the cytotoxic result to a mammalian cancer cell suggests their potential to be an effective treatment against tumor progression. Our analysis of the transcriptome suggests future studies to extend possibility of InP/ZnS QDs for controlling tumor proliferation and metastasis. The lack of effect to fibroblast cells is notable for clinical applications. Going forward, studies should further investigate treatment to non-cancerous tissues to assess use in cancer therapy. A direct comparison of Cd and InP/ZnS treated cells will also be valuable in identifying which QD exerts greater toxicity. Additionally, comparison of different sized InP/ZnS QDs can also be useful in determining the most effective for treatment options.

$$Y = \text{Min} + \frac{\text{Max} - \text{Min}}{1 + \left(\frac{X}{\text{IC}_{50}}\right)^{\text{Hill coefficient}}}$$

**Equation 1. Inhibition Concentration 50% (IC<sub>50</sub>)** Equation form used on AAT Bioquest website (<https://www.aatbio.com/tools/ic50-calculator>) to calculate IC<sub>50</sub> value. This value was used in following experiments as the tested treatment concentration.



**Table 1. Median Fluorescent Intensity** measuring viable HeLa cells positive for reactive oxygen species (ROS) production. Value indicates median fluorescent intensity of each sample (done in triplicate): non treated control without dye (NTC-), NTC with dye (NTC+), 69  $\mu\text{g}/\text{mL}$  InP/ZnS and 167  $\mu\text{g}/\text{mL}$  InP/ZnS. Two dyes used to measure two molecules of ROS: peroxynitrite by DHR, and superoxide by DHE.

<b>SAMPLE</b>	<b>DHR</b>	<b>DHE</b>
NTC-	18895	31636
	4600	50699
	0	47372
NTC+	2258	24078
	2445	19419
	2736	24810
69 $\mu\text{g}/\text{mL}$	32128	38506
	28511	39040
	34287	36109
167 $\mu\text{g}/\text{mL}$	37152	36938
	39439	42238
	30392	49376

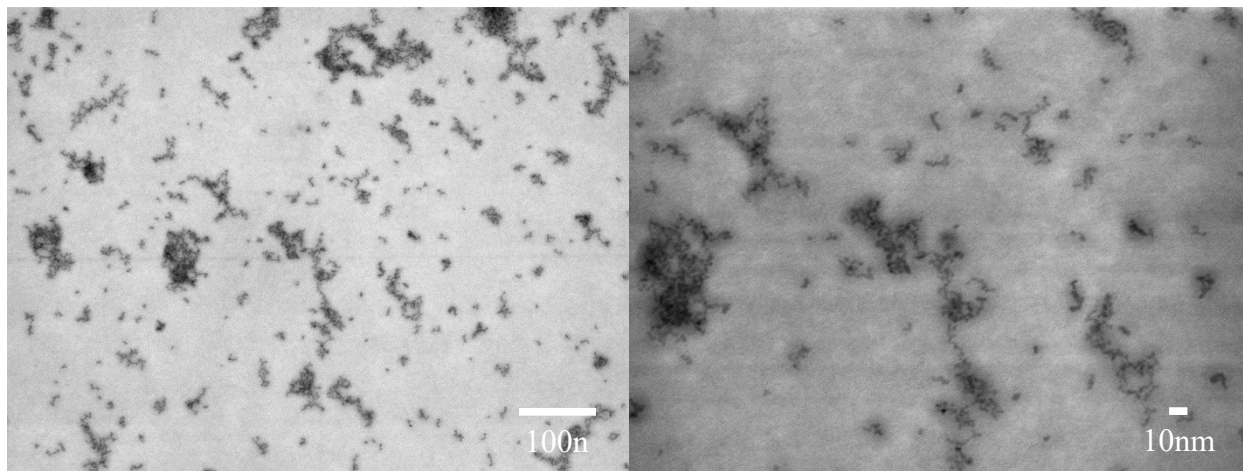


**Figure 1. STEM images of InP/ZnS (530nm) at low (left) and high (right) magnifications.**

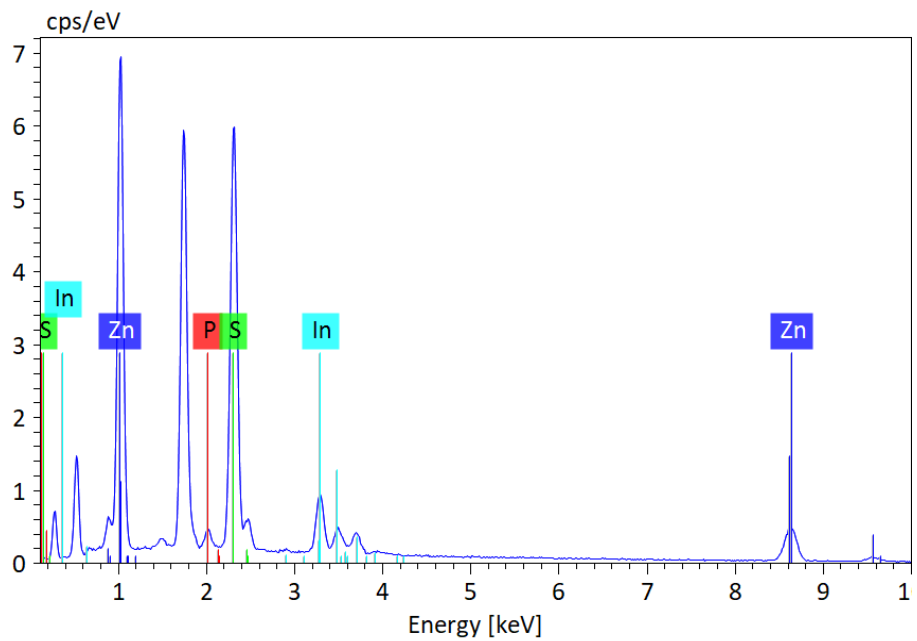


**Figure 2. EDAX spectra of InP/ZnS (530nm) QD to verify elemental composition.**

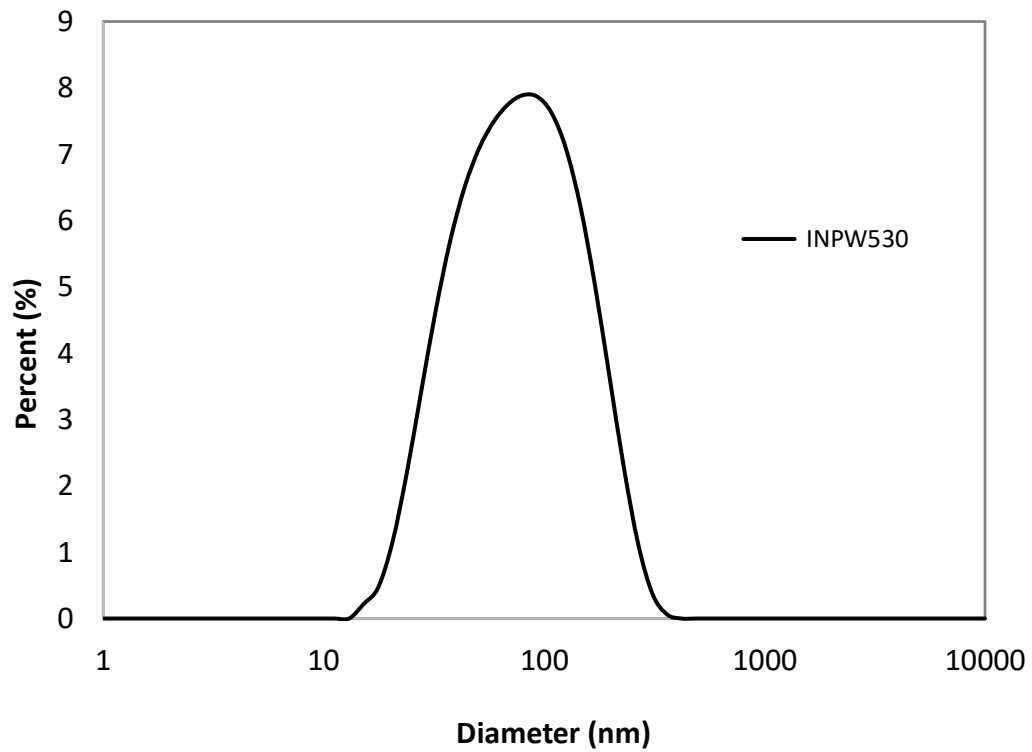


**Figure 3. Intensity size distribution** of INPW530 obtained by Dynamic Light Scattering

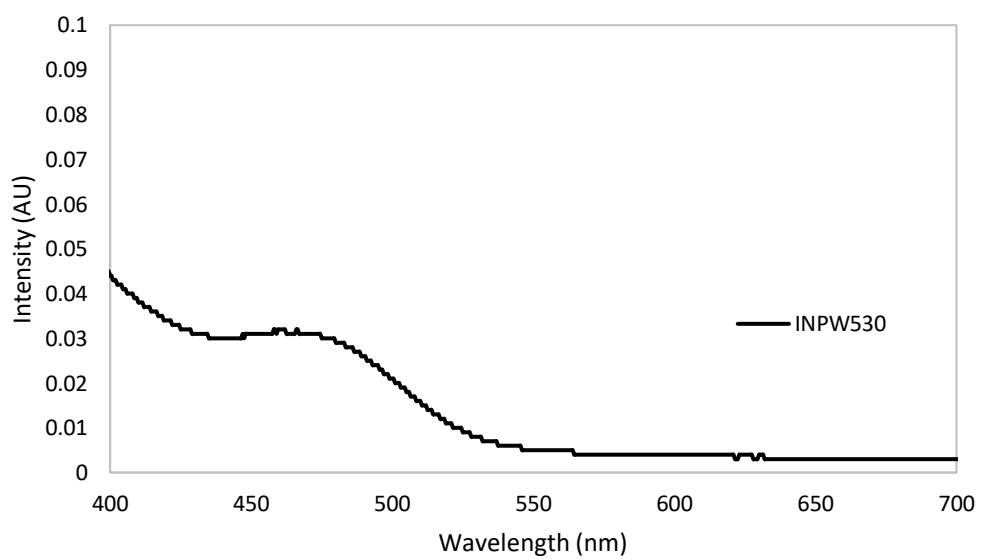
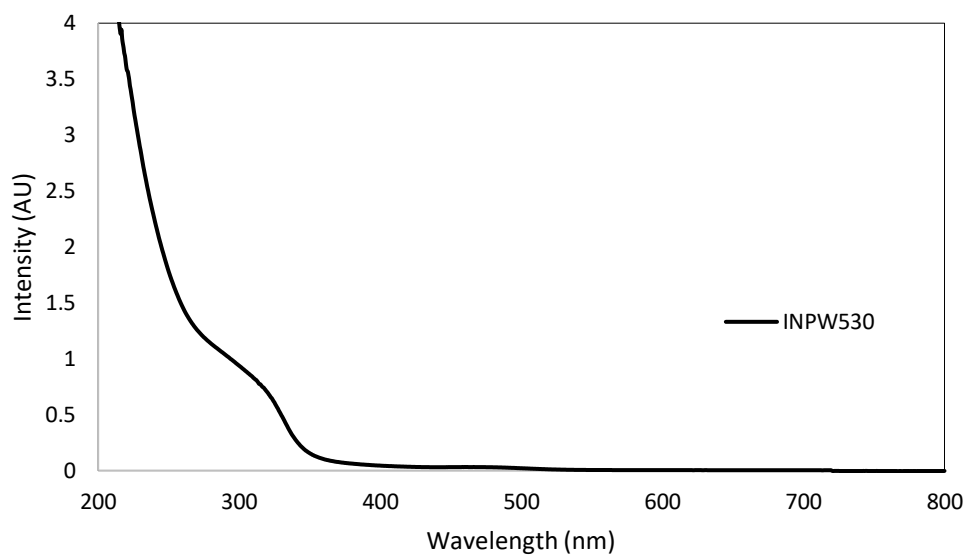


**Figure 4. UV-Vis absorption spectra of INPW530 (a) Full spectra; (b) Spectra for wavelength range of 400 to 700nm.**

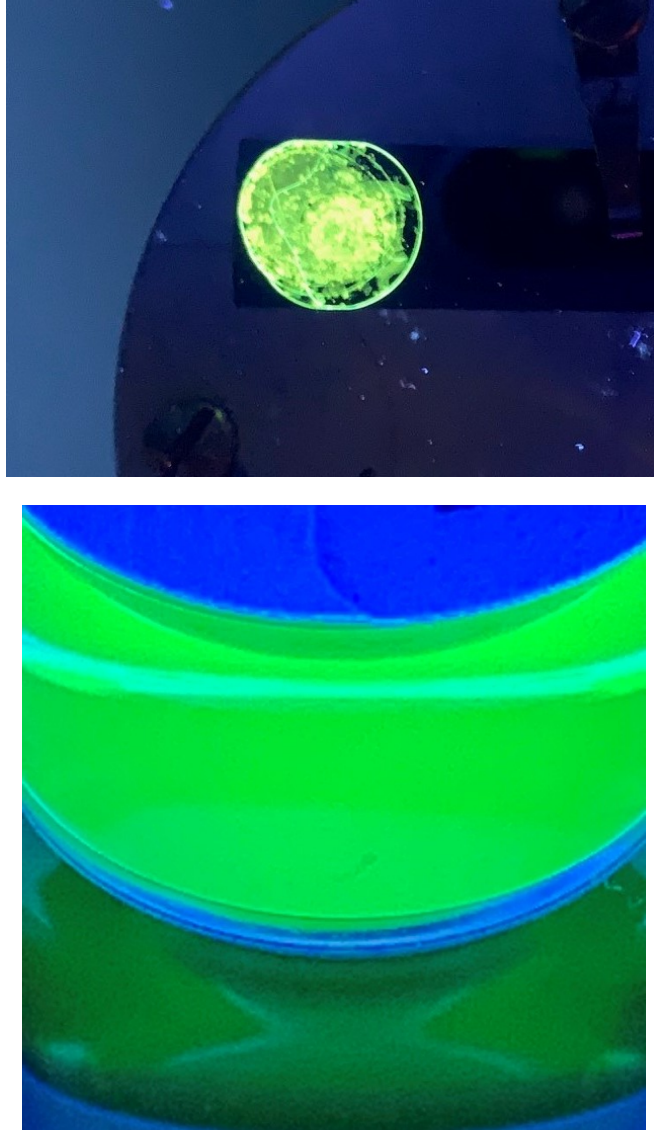
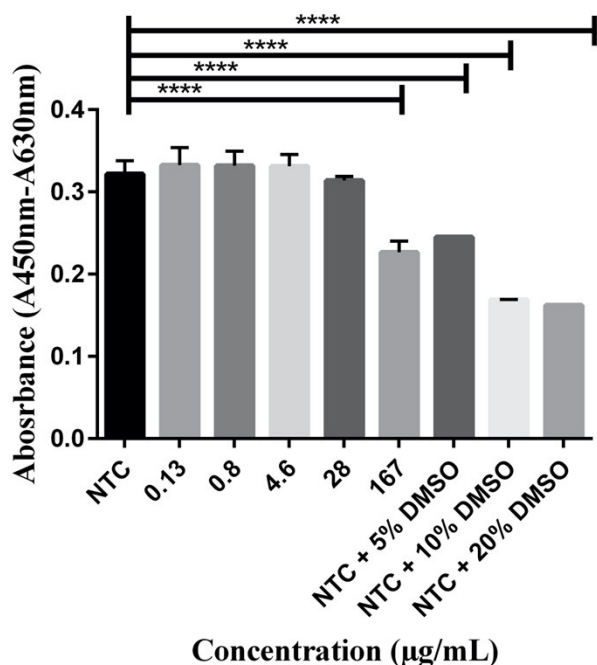


**Figure 5.** UV (365nm) light excitation of InP/ZnS QDs 530nm (green) on silicon substrates (top) and in liquid (bottom).

(A)

### Absorbance of HeLa cells Treated with InP/ZnS After 7 hours



(B)

### Absorbance of Fibroblasts Treated with InP/ZnS After 7 hr

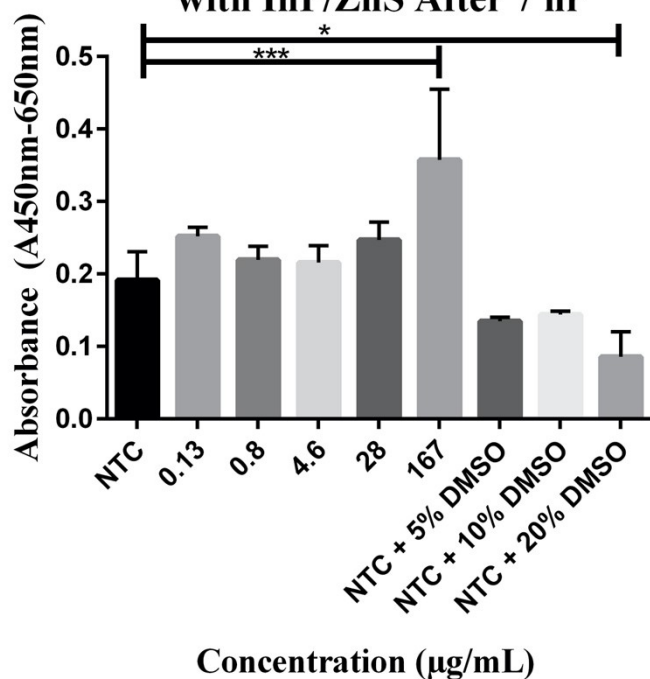


**Figure 6. Effects of InP/ZnS QD on cell viability measured by XTT reagents. (A)** HeLa cells show minor reduction in cell viability shown through 28  $\mu\text{g}/\text{mL}$  and significant reduction at 167  $\mu\text{g}/\text{mL}$ . Positive control with DMSO treatment shows statistically significant reduction in viability at higher percentages of DMSO. **(B)** Fibroblast cells have no significant decrease at all InP/ZnS concentration treatments (\* =  $p < 0.05$ , \*\*\*\* =  $p < 0.0001$ ).

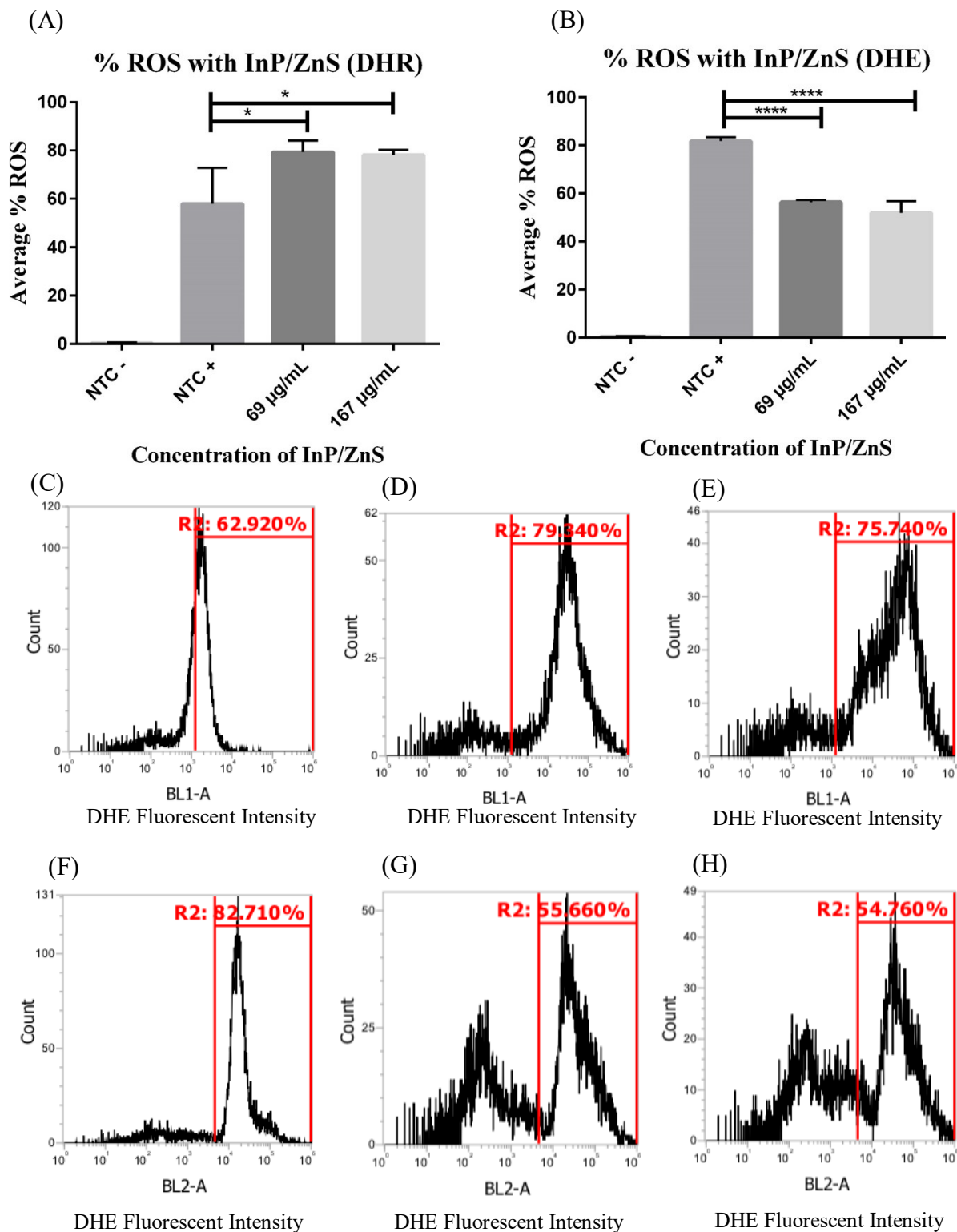


**Figure 7. ROS measurements with both DHE and DHR at varied InP/ZnS QD concentrations:** (A and B): Bar graphs comparing average percentages of ROS positive cells when dyed with DHE and DHR, respectively. Non-treated controls shown without (NTC-) and with (NTC+) dye. (C-E): Flow cytometer peaks taken from ROS Assay of samples dyed with DHR. A second, larger peak represents ROS production. (C) dyed, untreated control. (D) dyed sample treated with 69  $\mu\text{g/mL}$  InP/ZnS. (E) sample treated with 167  $\mu\text{g/mL}$  InP/ZnS. (F-H) Peaks of samples dyed with DHE. (F) dyed, untreated control. (G) dyed sample treated with 69  $\mu\text{g/mL}$  InP/ZnS. (H) dyed sample treated with 167  $\mu\text{g/mL}$  InP/ZnS. (\* =  $p < 0.05$ , \*\*\*\* =  $p < 0.0001$ )



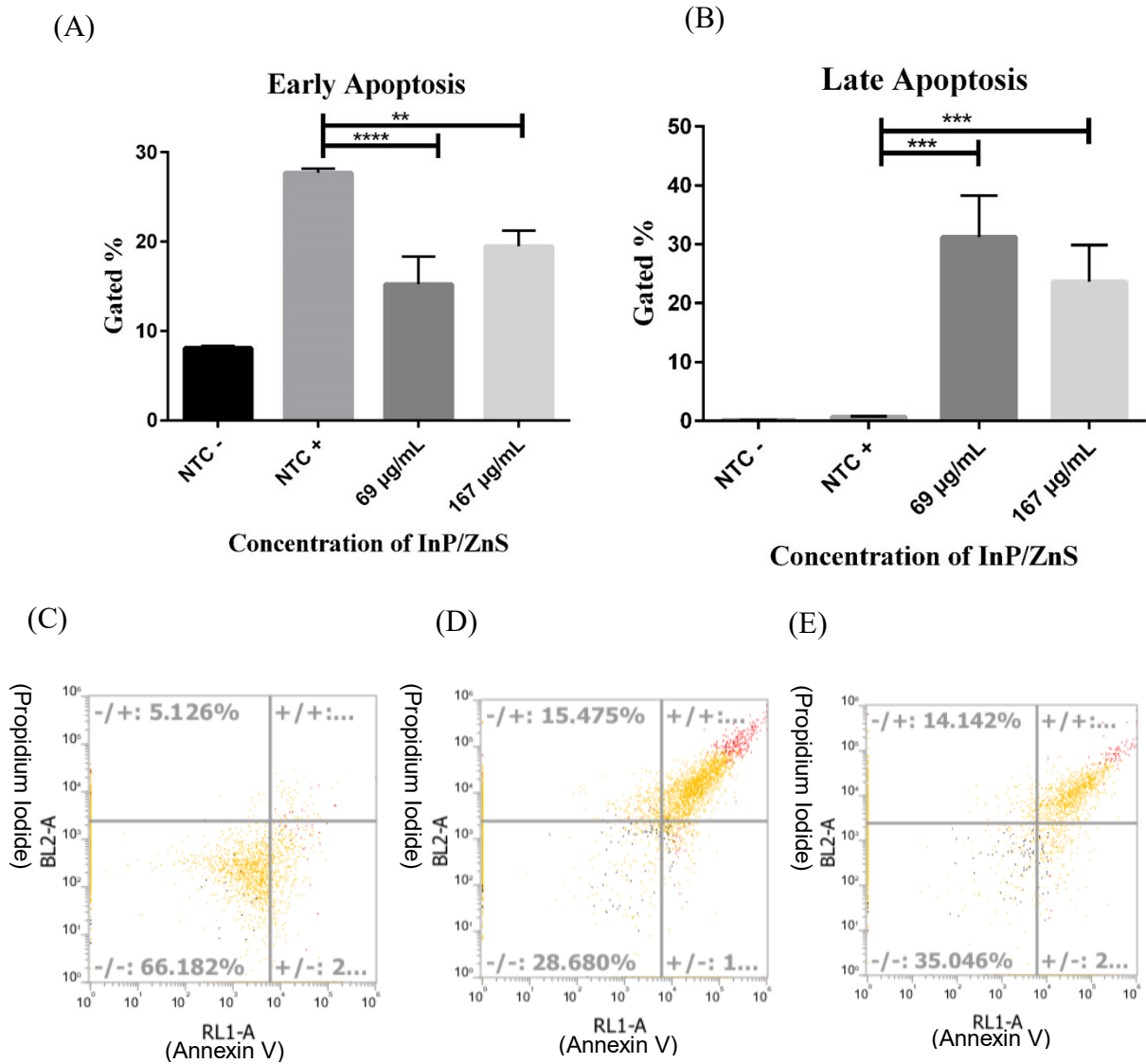
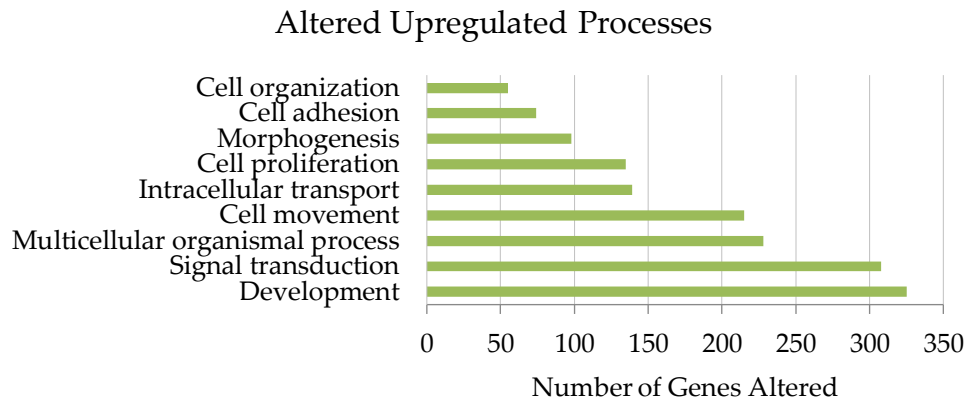


**Figure 8. Levels of early and late apoptosis after InP/ZnS treatment:** (A and B): Bar graph illustrating percent of apoptosis recorded by flow cytometer in samples treated with varying concentrations of InP/ZnS. NTC- represents non-treated control without dye and NTC+ is with dye. (C-E) Flow cytometer images of gated apoptosis levels. Each quadrant represents a stage of apoptosis: -/- control, ++ late apoptosis, and +/- early apoptosis. © represents dyed control group, (D) represents 69 µg/mL of InP/ZnS, and (E) represents 167 µg/mL of InP/ZnS. Error bars indicate standard deviation of samples. Statistically significant results are indicated based on P-values: \*  $p < 0.05$ , \*\*  $p < 0.01$ , \*\*\*  $p < 0.001$ , \*\*\*\*  $p < 0.0001$ .

(A)



(B)

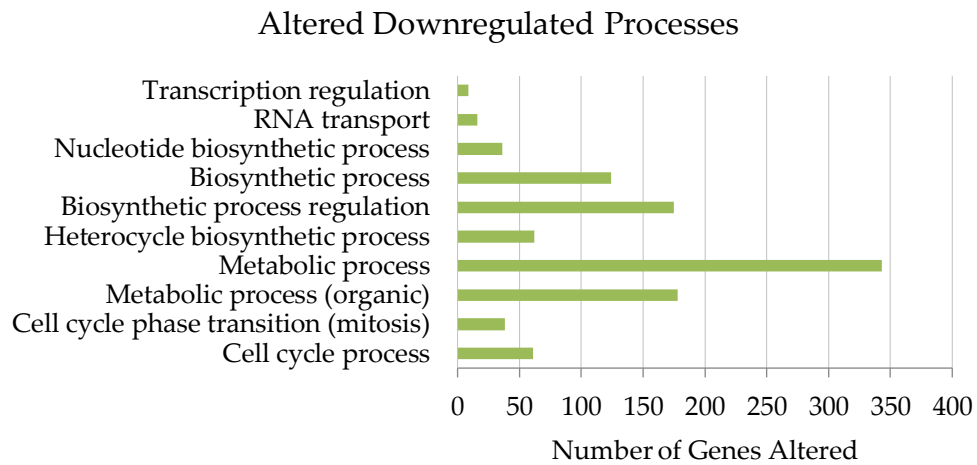


**Figure 9. Altered up and down regulated processes:** Bar graph representing number of genes upregulated (A) and downregulated (B), based on having p-value < 0.05. Genes grouped by common processes.

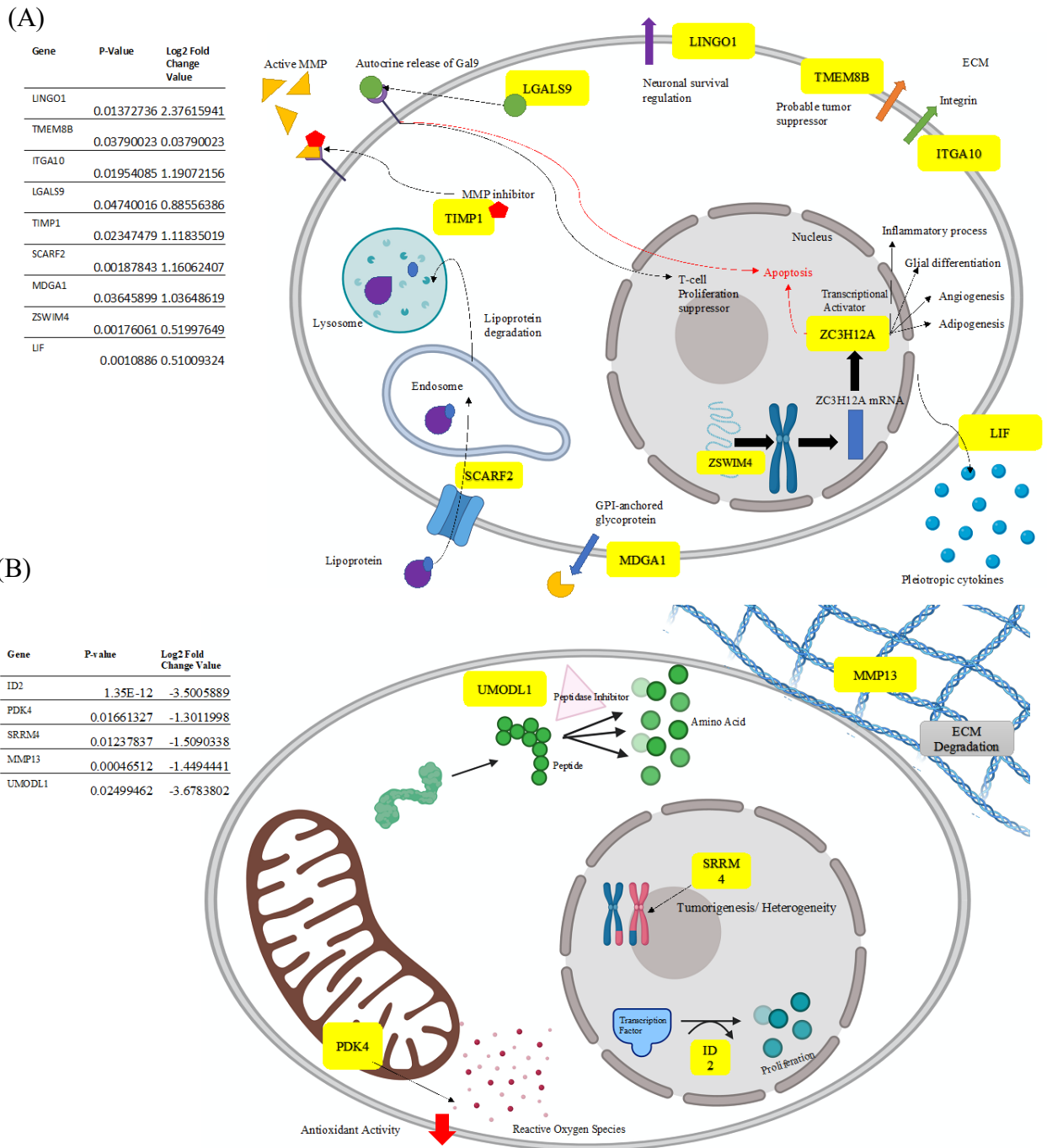


**Figure 10, A and B: Visualization of altered processes in the presence of InP/ZnS.**

Upregulated processes (A) observe evidence of metastatic inhibition, apoptosis due to autocrine release, and cytokine release. Downregulated processes (B) show pathways involving proliferation inhibition, increased ROS production, and varying levels of degradation. To the left of each model is a chart depicting each gene involved, along with the corresponding Log2 Fold Change value and P-value found with transcriptome analysis.

## REFERENCES

1. Lucey, B. P.; Nelson-Rees, W. A.; Hutchins, G. M. Henrietta Lacks, HeLa cells, and cell culture contamination. *Arch Pathol Lab Med.* **2019**, *133*, 1463-1467. <https://doi.org/10.1043/1543-2165-133.9.1463>.
2. Leighton, J. Contributions of tissue culture studies to an understanding of the biology of cancer: A review. *Cancer Res.* **1957**, *10*, 929–941.
3. Skloot, R. *The immortal life of Henrietta Lacks*. Broadway Paperbacks: New York, USA, **2011**.
4. Matea, C. T.; Mocan, T.; Tabaran, F.; Pop, T.; Mosteanu, O.; Puia, C.; Ian, C.; Mocan, L. Quantum dots in imaging, drug delivery and sensor applications. *Int J Nanomedicine.* **2017**, *12*, 5421-5431. <https://doi.org/10.2147/IJN.S138624>.
5. Michalet, X.; Pinaud, F. F.; Bentolila, L. A.; Tsay, J. M.; Doose, S.; Li, J. J.; Sundaresan, G.; Wu, A.; Gambhir, S.; Weiss, S. Quantum dots for live cells, in vivo imaging, and diagnostics. *Science.* **2005**, *307*, 538-544. <https://doi.org/10.1126/science.1104274>.
6. Deerinck, T. J. The application of fluorescent quantum dots to confocal, multiphoton, and electron microscopic imaging. *Toxicol Pathol.* **2008**, *36*, 112-116. <https://doi.org/10.1177/0192623307310950>.
7. Juzenas, P.; Chen, W.; Sun, Y. P.; Coelho, M. A. N.; Generalov, R.; Generalova, N.; Christensen, I. Quantum dots and nanoparticles for photodynamic and radiation therapies of cancer. *Adv Drug Deliv Rev.* **2018**, *60*, 1600-1614. <https://doi.org/10.1016/j.addr.2008.08.004>.
8. Liu, Q.; Zheng, C.; Zhao, H.; Wang, K.; Tao, W. Tumor cell pH detection based on CdSe quantum dots' fluorescence characteristics. *Technol Health Care.* **2019**, *27*, 239–247. <https://doi.org/10.3233/THC-199023>.
9. Zhang, T.; Wang, Y.; Kong, L.; Xue, Y.; Tang, M. Threshold dose of three types of quantum dots (QDs) induces oxidative stress triggers DNA damage and apoptosis in mouse fibroblast L929 cells. *Int J Environ Res Public Health.* **2015**, *12*, 13435-13454. <https://doi.org/10.3390/ijerph121013435>.
10. Kim, M. W.; Jeong, H. Y.; Kang, S. J.; Choi, M. J.; You, Y. M.; Im, C. S.; Lee, T.; Song, I.; Lee, C.; Rhee, K. et. al. Cancer-targeted nucleic acid delivery and quantum dot imaging using EGF receptor aptamer-conjugated lipid nanoparticles. *Sci Rep.* **2017**, *7*, 9474. <https://doi.org/10.1038/s41598-017-09555-w>.
11. Christensen, J.; Vonwil, D.; Prasad, V. S. Non-invasive in vivo imaging and quantification of tumor growth and metastasis in rats using cells expressing far-red fluorescence protein. *PLoS ONE.* **2015**, *10*, 1–14. <https://doi.org/10.1371/journal.pone.0132725>.

12. Zheng, H.; Li, X.; Chen, C.; Chen, J.; Sun, J.; Sun, S.; Jin, L.; Li, J.; Sun, S.; Wu, Z. Quantum dot-based immunofluorescent imaging and quantitative detection of TOP2A and prognostic value in triple-negative breast cancer. *Int J Nanomedicine*. **2016**, *11*, 5519-5529. <https://doi.org/10.2147/IJN.S111594>.
13. Liu, S. L.; Zhang, L. J.; Wang, Z. G.; Zhang, Z. L.; Wu, Q. M.; Sun, E. Z.; She, Y.; Pang, D. Globally visualizing the microtubule-dependent transport behaviors of influenza virus in live cells. *Anal Chem*. **2014**, *86*, 3902–3908. <https://doi.org/10.1021/ac500640u>.
14. Fang, M.; Peng, C. W.; Pang, D. W.; Li, Y. Quantum dots for cancer research: current status, remaining issues, and future perspectives. *Cancer Bio Med*. **2012**, *9*, 151–163. <https://doi.org/10.7497/j.issn.2095-3941.2012.03.001>.
15. Zhu, C.; Chen, Z.; Gao, S.; Goh, B. L.; Samsudin, I.; Lwe, K.; Wu, Y.; Wu, C.; Su, X. Recent advances in non-toxic quantum dots and their biomedical applications. *Prog Nat Sci: Mat Int*. **2019**, *29*, 628–640. <https://doi.org/10.1016/j.pnsc.2019.11.007>.
16. Hens, B.; Smothers, J.; Rizvanovic, H.; Patel, R.; Wu, Q.; Kim, K. The future of anticancer drugs: A cytotoxicity assessment study of CdSe/ZnS quantum dots. *J Nanotheranostics*. **2020**, *1*, 19-38. <https://doi.org/10.3390/jnt1010003>.
17. Lim, S. J.; Ma, L.; Schleife, A.; Smith, A. M. Quantum dot surface engineering: Toward inert fluorophores with compact size and bright, stable emission. *Coord Chem Rev*. **2016**, *320-321*, 216-237. <https://doi.org/10.1016/j.ccr.2016.03.012>.
18. Zhang, L. W.; Monteiro-Riviere, N. A. Mechanisms of quantum dot nanoparticle cellular uptake. *Toxicol Sci*. **2009**, *110*, 138-155. <https://doi.org/10.1093/toxsci/kfp087>.
19. Lin, G.; Chen, T.; Pan, Y.; Yang, Z.; Li, L.; Yong, K. T. Biodistribution and acute toxicity of cadmium-free quantum dots with different surface functional groups in mice following intratracheal inhalation. *Nanotheranostics*. **2020**, *4*, 173-183. <https://doi.org/10.7150/ntno.42786>.
20. Chen, Ting; Li, L.; Xu, G.; Wang, X.; Wang, J.; Chen, Y.; Jiang, W.; Yang, Z.; Lin, G. Cytotoxicity of InP/ZnS quantum dots with different surface functional groups toward two lung-derived cell lines. *Front Pharmacology*. **2018**, *9*, 763. <https://www.ncbi.nlm.nih.gov/pmc/articles/PMC6053512/>.
21. Roberts, J. R.; Antonini, J. M.; Porter, D. W.; Chapman, R. S.; Scabilloni, J. F.; Young, S. H.; Schwegler-Berry, D.; Castranova, V.; Mercer, R. Lung toxicity and biodistribution of Cd/Se-ZnS quantum dots with different surface functional groups after pulmonary exposure in rats. *Part Fibre Toxicol*. **2013**, *10*, 5. <https://doi.org/10.1186/1743-8977-10-5>.
22. Wang, M.; Wang, J.; Sun, H.; Han, S.; Feng, S.; Shi, L.; Meng, P.; Li, J.; Huang, P.; Sun, Z. Time-dependent toxicity of cadmium telluride quantum dots on liver and kidneys in mice: Histopathological changes with elevated free cadmium ions and hydroxyl radicals. *Int J Nanomedicine*. **2016**, *11*, 2319-2328. <https://doi.org/10.2147/IJN.S103489>.

23. Su, Y.; He, Y.; Lu, H.; Sai, L.; Li, Q.; Li, W.; Wang, L.; Shen, P.; Huang, Q.; Fan, C. The cytotoxicity of cadmium based, aqueous phase - Synthesized, quantum dots and its modulation by surface coating. *Biomaterials*. **2009**, *30*, 19-25. <https://doi.org/10.1016/j.biomaterials.2008.09.029>.
24. Williams, D. N.; Pramanik, S.; Brown, R. P.; Zhi, B.; McIntire, E.; Hudson-Smith, N. V.; Haynes, C.; Rosenzweig, Z. Adverse interactions of luminescent semiconductor quantum dots with liposomes and shewanella oneidensis. *ACS Appl Nano Mater*. **2018**, *9*, 4788-4800. <https://doi.org/10.1021/acsnm.8b01000>.
25. Horstmann, C.; Kim, D. S.; Campbell, C.; Kim, K. Transcriptome profile alteration with cadmium selenide/zinc sulfide quantum dots in *Saccharomyces cerevisiae*. *Biomol*. **2019**, *9*, 653. <https://doi.org/10.3390/biom9110653>.
26. Ayupova, D.; Dobhal, G.; Laufersky, G.; Nann, T.; Goreham, R. V. An in vitro investigation of cytotoxic effects of InP/ZnS quantum dots with different surface chemistries. *Nanomaterials*. **2019**, *9*, 135. <https://doi.org/10.3390/nano9020135>.
27. Chen, S.; Chen, Y.; Chen, Y.; Yao, Z. InP/ZnS quantum dots cause inflammatory response in macrophages through endoplasmic reticulum stress and oxidative stress. *Int J Nanomedicine*. **2019**, *14*, 9577-9586. <https://doi.org/10.2147/IJN.S218748>.
28. Ziental, D.; Czarczynska-Goslinska, B.; Mlynarczyk, D. T.; Glowacka-Sobotta, A.; Stanis, B.; Goslinski, T.; Mlynarczyk, D.; Sobota, A.; Stanis, B.; Goslinski, T.; Sobotta, L. Titanium Dioxide Nanoparticles: Prospects and Applications in Medicine. *Nanomaterials*. **2020**, *10*, 387. [10.3390/nano10020387](https://doi.org/10.3390/nano10020387).
29. Di Meo, S.; Reed, T. T.; Venditti, P.; Victor, V. M. Role of ROS and RNS Sources in Physiological and Pathological Conditions. *Oxid Med Cellular Longevity*. **2016**. <https://doi.org/10.1155/2016/1245049>.
30. Dai, D.-F.; Chiao, Y.; Marcinek, D. J.; Szeto, H. H.; Rabinovitch, P. S. Mitochondrial oxidative stress in aging and healthspan. *Longevity & Healthspan*. **2014**, *3*, 6. <https://doi.org/10.1186/2046-2395-3-6>.
31. Radi, R. Oxygen radicals, nitric oxide, and peroxynitrite: Redox pathways in molecular medicine. *Proc Natl Acad Sci U S A*. **2018**, *115*, 5839-5848. <https://doi.org/10.1073/pnas.1804932115>.
32. Redza-Dutordoir, M.; Averill-Bates, D. A. Activation of apoptosis signaling pathways by reactive oxygen species. *Biochim Biophys Acta Mol Cell Res*. **2016**, *1863*, 2977-2992. <https://doi.org/10.1016/j.bbamcr.2016.09.012>.
33. Kaczanowski, S. Apoptosis: Its origin, history, maintenance and the medical implications for cancer and aging. *Phys Biol*. **2016**, *13*, 3. <https://doi.org/10.1088/1478-3975/13/3/031001>.

34. Elmore, S. Apoptosis: A review of programmed cell death. *Toxicol Pathol.* **2007**, *35*, 495-516. <https://doi.org/10.1080/01926230701320337>.
35. Fan, F.; Jin, S.; Amundson, S. A.; Tong, T.; Fan, W.; Zhao, H.; Zhu, X.; Mazzacurati, L.; Li, X.; Petrik, K. et. al. ATF3 induction following DNA damage is regulated by distinct signaling pathways and over-expression of ATF3 protein suppresses cells growth. *Oncogene.* **2002**, *49*, 7488–7496. <https://doi.org/10.1038/sj.onc.1205896>.
36. Moussa, H.; Merlin, C.; Dezanet, C.; Balan, L.; Medjahdi, G.; Ben-Attia, M.; Schneider, R. Trace amounts of CU<sup>2+</sup> ions influence ROS production and cytotoxicity of ZnO quantum dots. *J Hazard Mater.* **2016**, *304*, 532-542. <https://doi.org/10.1016/j.jhazmat.2015.11.013>.
37. Owusu, E. G. A.; Naasani, I.; Parkin, I. P.; Allan, E.; Yaghini, E. Photoactivable polymers embedded with Cadmium-Free Quantum Dots and crystal violet: Efficient bactericidal activity against clinical strains of antibiotic-resistant bacteria. *ACS App. Mater. Interfaces.* **2019**, *11*, 12367-12378. <https://doi.org/10.1021/acsami.9b02109>.
38. Chibli, H.; Carlini, L.; Park, S.; Dimitrijevic, N. M.; Nadeau, J. L. Cytotoxicity of InP/ZnS quantum dots related to reactive oxygen species generation. *Nanoscale.* **2011**, *3*, 2552-2559. <https://doi.org/10.1039/c1nr10131e>.
39. Corce, V.; Chamoreau, L. M.; Derat, E.; Goddard, J. P.; Ollivier, C.; Fensterbank, L. Silicates as latent alkyl radical precursors: Visible-light photocatalytic oxidation of hypervalent bis-catecholato silicon compounds. *Agew Chem Int Ed.* **2015**, *39*, 11414-11418. <https://doi.org/10.1002/anie.201504963>.
40. Wu, T.; Liang, X.; He, K.; Liu, X.; Li, Y.; Wang, Y.; Kong, L.; Tang, M. The NLRP3-mediated neuroinflammatory responses to CdTe quantum dots and the protection of ZnS shell. *Int Jo Nanomed.* **2020**, *15*, 3217–3233. <https://doi.org/10.2147/IJN.S246578>.
41. Abdul-Sater, A. A.; Koo, E.; Häcker, G.; Ojcius, D. M. Inflammasome-dependent caspase-1 activation in cervical epithelial cells stimulates growth of the intracellular pathogen Chlamydia trachomatis. *J Biol Chem.* **2009**, *284*, 26789–26796. <https://doi.org/10.1074/jbc.M109.026823>.
42. Fujita, K.; Iwama, H.; Oura, K.; Tadokoro, T.; Samukawa, E.; Sakamoto, T.; Nomura, T.; Tani, J.; Yoneyama, H.; Morishita, A. et. al. Cancer therapy due to apoptosis: Galectin-9. *Int J Mol Sci.* **2017**, *18*, 1–15. <https://doi.org/10.3390/ijms18010074>.
43. Holderried, T. A. W.; De Vos, L.; Bawden, E. G.; Vogt, T. J.; Dietrich, J.; Zarbl, R.; Boots, F.; Kristiansen, G.; Brossart, P.; Landsberg, J.; Dietrich, D. Molecular and immune correlates of TIM-3 (HAVCR2) and galectin 9 (LGALS9) mRNA expression and DNA methylation in melanoma. *Clin Epigenetics.* **2019**, *11*, 161. <https://doi.org/10.1186/s13148-019-0752-8>.



44. Chen, Tao; Du, D.; Chen, J.; Zhou, P.; Weinstein, J. N.; Yao, L.; Yuexin, L. ZC3H12A expression in different stages of colorectal cancer. *Oncoscience*. **2018**, *6*, 301-311. <https://doi.org/10.18632/oncoscience.480>.
45. Vazquez, J. M.; Sulak, M.; Chigurupati, S.; Lynch, V. J. A zombie LIF gene in elephants is upregulated by TP53 to induce apoptosis in response to DNA damage. *Cell Rep*. **2018**, *24*, 1765-1776. <https://doi.org/10.1016/j.celrep.2018.07.042>.
46. Saftencu, M.; Braicu, C.; Cojocneanu, R.; Buse, M.; Irimie, A.; Piciu, D.; Berindan-Neagoe, I. Gene expression patterns unveil new insights in papillary thyroid cancer. *Medicina (Lithuania)*. **2019**, *55*, 500. <https://doi.org/10.3390/medicina55080500>.
47. Dumortier, M.; Ladam, F.; Damour, I.; Vacher, S.; Bièche, I.; Marchand, N.; Launoit, Y.; Tulasne, D.; Chotteau-Lelievre, A. ETV4 transcription factor and MMP13 metalloprotease are interplaying actors of breast tumorigenesis. *Breast Cancer Res*. **2018**, *20*, 73. <https://doi.org/10.1186/s13058-018-0992-0>.
48. Zhang, W.; Zhang, S. L.; Hu, X.; Tam, K. Y. Targeting tumor metabolism for cancer treatment: Is pyruvate dehydrogenase kinases (PDKs) a viable anticancer target? *Int J Biol Sci*. **2015**, *11*, 1390-1400. <https://doi.org/10.7150/ijbs.13325>.
49. Taggart, K.; Estrada, A.; Thompson, P.; Lourenco, F.; Kirmani, S.; Suzuki-Hatano, S.; Pacak, C. PDK4 deficiency induces intrinsic apoptosis in response to starvation in fibroblasts from doberman pinschers with dilated cardiomyopathy. *BioResearch Open Access*. **2017**, *6*, 182–191. <https://doi.org/10.1089/biores.2017.0023>.
50. Ameri, K.; Jahangiri, A.; Rajah, A. M.; Tormos, K. V.; Nagarajan, R.; Pekmezci, M.; Nguyen, V.; Wheeler, M.; Murphy, M.; Sanders, T. HIGD1A regulates oxygen consumption, ROS production, and AMPK activity during glucose deprivation to modulate cell survival and tumor growth. *Cell Rep*. **2015**, *10*, 891–899. <https://doi.org/10.1016/j.celrep.2015.01.020>.
51. Chanrion, M.; Negre, V.; Fontaine, H.; Salvetat, N.; Bibeau, F.; Mac Grogan, G.; Mauriac, L.; Katsaros, D.; Molina, F.; Theillet, C.; Darbon, J. A gene expression signature that can predict the recurrence of tamoxifen-treated primary breast cancer. *Clin Cancer Res*. **2008**, *6*, 1744–1752. <https://doi.org/10.1158/1078-0432.CCR-07-1833>.
52. Roszik, J.; Ring, K. L.; Wani, K. M.; Lazar, A. J.; Yemelyanova, A. V.; Soliman, P. T.; Frumovitz, M.; Jazaeri, A. Gene expression analysis identifies novel targets for cervical cancer therapy. *Front Immunol*. **2018**, *9*, 2102. <https://doi.org/10.3389/fimmu.2018.02102>.
53. Liu, Y.; Pandey, P. R.; Sharma, S.; Xing, F.; Wu, K.; Chittiboyina, A.; Wu, S.; Tyagi, A.; Watabe, K. ID2 and GJB2 promote early-stage breast cancer progression by regulating cancer stemness. *Breast Cancer Res Treat*. **2019**, *175*, 77-90. <https://doi.org/10.1007/s10549-018-05126-3>.



54. Lee, S. B.; Frattini, V.; Bansal, M.; Castano, A. M.; Sherman, D.; Hutchinson, K.; Bruce, J.; Califano, A.; Liu, G.; Cardozo, T. et. al. An ID2-dependent mechanism for VHL inactivation in cancer. *Nature*. **2016**, *529*, 172-177. <https://doi.org/10.1038/nature16475>.
55. Shimojo, M.; Kasahara, Y.; Inoue, M.; Tsunoda, S.; Shudo, Y.; Kurata, T.; Obika, S. A gapmer antisense oligonucleotide targeting SRRM4 is a novel therapeutic medicine for lung cancer. *Sci Rep*. **2019**, *9*, 7618. <https://doi.org/10.1038/s41598-019-43100-1>.
56. Ohnishi, T.; Shirane, M.; Nakayama, K. I. SRRM4-dependent neuron-specific alternative splicing of protrudin transcripts regulates neurite outgrowth. *Sci Rep*. **2017**, *7*, 41130. <https://doi.org/10.1038/srep41130>.
57. Lee, A. R.; Gan, Y.; Tang, Y.; Dong, X. A novel mechanism of SRRM4 in promoting neuroendocrine prostate cancer development via a pluripotency gene network. *EBioMedicine*. **2018**, *35*, 167-177. <https://doi.org/10.1016/j.ebiom.2018.08.011>.
58. Tan, Q.; Cui, J.; Huang, J.; Ding, Z.; Lin, H.; Niu, X.; Li, Z.; Wang, G.; Luo, Q.; Lu, S. Genomic alteration during metastasis of lung adenocarcinoma. *Cell Physiol Biochem*. **2016**, *38*, 469-486. <https://doi.org/10.1159/000438644>.
59. Wang, G.; Liu, X.; Xie, J.; Meng, J.; Ni, X. PDK-1 mediated Hippo–YAP–IRS2 signaling pathway and involved in the apoptosis of non-small cell lung cancer cells. *Biosci Rep*. **2019**, *39*, 5. <https://doi.org/10.1042/BSR20182099>.
60. Martin, M. D.; Matrisian, L. M. The other side of MMPs: Protective roles in tumor progression. *Cancer Metastasis Rev*. **2017**, *26*, 717-724. <https://doi.org/10.1007/s10555-007-9089-4>.